Q. J. R. Meteorol. Soc. (1999), **125**, pp. 2937–2963

Tropical-wide teleconnection and oscillation. II: The ENSO–monsoon system

By K. MIYAKODA, A. NAVARRA* and M. N. WARD†
Istituto per lo studio delle Metodologie Geofisiche Ambientali, Italy

(Received 4 August 1997; revised 26 January 1999)

SUMMARY

Two teleconnection indices, discussed in Part I, i.e. the Tropical-wide Oscillation Index (TOI) and the Walker circulation Index (WAI), are applied to the analysis of the ENSO–monsoon (El Niño Southern Oscillation–Asian monsoons) system. The first hypothesis presented in Part I was that the TOI for July–August–September (JAS) is closely related to the Indian summer monsoon index as well as the Southern Oscillation Index. As a result, the TOI represents the lead–lag characteristics of the tropical circulation variability over the eastern hemisphere (45°E–170°E) and simultaneously its interaction with the ENSO over the equatorial Pacific. The second hypothesis was that there are two types of connection between the ENSO and Asian monsoons: type I with distinct connection in space and time, and type II without connection. The WAI provides a measure for this connection. This idea is supported by comparisons of observed and model teleconnection structures in Part I.

Part II investigates these relations further. Time–lag correlations are calculated between the key indices and atmospheric variables over the equatorial Indo-Pacific Oceans. If type II years, derived by the WAI, are removed from the 34-year time series, correlations between the TOI and these variables increase appreciably, now showing clearly the biennial character. The analysis identifies a sequence of events involving biennial oscillation of the ENSO–monsoon system from approximately JAS(−1) to JAS(0), followed by intensification of the ENSO from JAS(0) to November–December–January(+1). The ENSO–monsoon oscillation system is not sinusoidal but skewed.

To show the geographical patterns associated with the above sequence of events, planar maps are presented of the lag correlation between the observed TOI(JAS) and (i) vertical velocity at the 500 hPa level, (ii) precipitation, (iii) sea surface temperature (SST), and (iv) atmospheric sea level pressure. Distinct geographical distributions of the ENSO–monsoon oscillation emerge in both the observations and model data. One pattern is characterized by a horseshoe shape over the Pacific, which is generally symmetric around the equator, but with geographical differences depending on location in the lag sequence. The other pattern is a see-saw shape, primarily a standing oscillation located in the eastern South Pacific and the Indian Oceans, resembling the sea-level-pressure pattern found by Trenberth and Shea. Applying the lead–lag relationship, it is demonstrated that the SST over the central Pacific four months ahead can be projected, based on the TOI(JAS). Conversely, the intensity of the Indian monsoon rainfall for non-type II years can be projected 15 months ahead by the SST over the eastern Pacific Ocean. This indicates that the ENSO–monsoon oscillation system is quasi-periodic, as opposed to irregular, with a two-year cycle; this is clearly revealed with the removal of type II years.

KEYWORDS: Asian summer monsoon ENSO General-circulation model

1. INTRODUCTION

It is assumed that the El Niño Southern Oscillation (ENSO) is a quasi-periodic oscillation, with warm/cold events in the equatorial Pacific as the two opposite extremes, and that the ENSO belongs to a larger system (Meehl 1987, 1994, 1997; Webster and Yang 1992). This larger system could be the Southern Oscillation (SO) or could be the Tropical-wide Oscillation (TO), which includes wet/dry events of the Asian summer monsoons, and wet/dry Sahel rainfall events as well. Links from the Indian monsoon to the ENSO have been extensively discussed (e.g. Mooley and Parthasarathy 1983, 1984), and there is a fair amount of evidence that the intensity of the Indian monsoon contains a precursory or simultaneous signal to the ENSO activity. The correlation coefficient between Indian monsoon rainfall (IMR) for June–July–August (JJA) and NINO3 sea surface temperature (SST) for 34 years is 0.64.

Research concerning the return cycle from the ENSO to the Asian monsoon has recently become more active. After Weare (1979), Khandekar (1979), Angell (1981), Mooley and Parthasarathy (1983, 1984), Rasmusson and Carpenter (1983) and Bhalme

* Corresponding author, present address: Center for Ocean–Land–Atmosphere Studies, 4041 Powder Mill Road, Calverton, MD 20705-3106, USA.
† Also affiliated to the University of Oklahoma, USA.

and Jadhav (1984), several papers discussed this topic, including Ropelewski and Halpert (1987, 1989), Nitta (1987), Brankovic *et al.* (1994), Ju and Slingo (1995), Shen and Lau (1995) (hereafter referred to as SL95), and Sperber and Palmer (1997). These studies all find that warm events of the ENSO tend to be associated with poor monsoon activity, and cold events of the ENSO are associated with a good monsoon.

2. Issues

In Part I (Navarra *et al.* 1999), two indices were selected as viable measures of atmospheric teleconnection between the ENSO and the Asian monsoons, and their teleconnectivities were investigated.

(*a*) *The Tropical-wide Oscillation Index (TOI)*

One of the indices is the TO index (TOI), which is defined by the empirical orthogonal function (EOF) mode 1 of normalized rainfall anomaly in the tropical belt between 40°N and 20°S. Particularly the TOI for the season July–August–September (JAS) denoted TOI(JAS). The conventional Indian summer monsoon index, IMR(JJA), corresponds to the rainfall intensity over the geographical maximum in the loading function of EOF 1 for JJA. Therefore, the TOI(JAS) and the IMR(JJA) are closely related. Yet it is likely that the time coefficients of the EOF 1, i.e. the TOI, are more stable in relating with other variables in the tropical zone than the IMR. Both the TOI(JAS) and the boreal winter index, the TOI for January–February-March (JFM), are broadly distributed, covering the equatorial Pacific and the Indian Ocean. But a crucial aspect is that the TOI(JAS) includes the Indian subcontinent (off equator) in its primary influence domain, while the TOI(JFM) does not. The TOI(JAS) embraces both the SO index (SOI) for JAS and the IMR(JAS); therefore, the TOI represents better the teleconnection of the ENSO–monsoon than the SOI or the IMR alone.

(*b*) *The Walker circulation Index (WAI)*

The second index proposed in Part I is the Walker circulation Index (WAI), which provides a measure of the coupling/decoupling mode for the ENSO and the monsoon connection. It is hypothesized that, if the ascending branch of the Walker circulation is located at its climatological (close-to-normal) position along the equator, the teleconnection is localized and the ENSO–monsoon connection remains weak (type II), whereas if the ascending branch of the Walker circulation is shifted sufficiently eastward or westward from its normal location, the teleconnection becomes strong and active (type I). The degree of the deviation of the ascending branch can be measured by EOF 1 of the SST anomaly distribution in the 10° latitudinal belt south of the equator in the Indian and Pacific Oceans.

The hypothesis of the Walker circulation arises from the analogy of a pendulum. If the pendulum in JAS is sufficiently shifted from the neutral position, the pendulum continues to oscillate for the rest of the year. On the other hand, if the pendulum is set in the neutral position, it does not oscillate. In Part I, some evidence was shown of the relationship between the ascending location of the Walker circulation and up/downdraught over India, and on the relation between the updraught position of the Walker circulation and the SST anomaly distribution along the Indo-Pacific equatorial belt (0°–10°S).

There is, however, a counter argument against the idea of type I/type II. The teleconnection is generated simply by a localized heat source associated with the ENSO. If this signal is strong enough to overcome the internal noise of the atmosphere, the

teleconnection emerges strongly. There is no demarkation between strong and weak SST anomalies. Which version is working in nature? Type I/type II separation or no additional demarkation rule? One of the aims of this paper is to discuss these points and to demonstrate the validity of the hypothesis of the Walker circulation. If the heat source associated with the ENSO is strong enough to overcome the internal noise, the teleconnection emerges strongly without any clear-cut demarkation. If true, this idea negates the WAI assumption. In this paper this point will be examined together with the further investigation of the two hypotheses.

(c) *The data of observation and model*

The observed data mainly used in this paper are: (i) Norwich's Climate Research Unit (CRU) gridded dataset of precipitation for 34 years, (ii) the UK Meteorological Office (UKMO) Global Sea Ice and SST (GISST) for 34 years, (iii) the blended data of precipitation by Xie–Arkin from 1979 to 1994, and (iv) the European Centre for Medium-Range Weather Forecasts (ECMWF) data-assimilation re-analysis (ERA) from 1981 to 1989.

The general-circulation model (GCM) data used here are: omega (the vertical pressure velocity) at 500 hPa level, precipitation and sea-level pressure for 34 years. All of them are obtained from simulations performed with an atmospheric GCM, ECHAM4 with triangular truncation at wave number 30 and with 19 vertical levels. The ECHAM4 is a climate GCM, which has evolved from the medium-range forecasting model at the ECMWF, but significantly modified at the Max-Planck Institute fur Meteorologie, Hamburg. Experiments were run with this model from 1961 to 1994. The lower-boundary conditions of the SST and ice boundary are given by the GISST data. See Part I for details.

3. TIME–LONGITUDE DIAGRAMS

(a) *SST lag correlation*

Figure 1 presents the correlation between the model TOI(JAS) and SST along the equatorial Indo-Pacific Oceans (10°N–10°S). On the abscissa there is longitude, and on the ordinate time, from -1 to $+1$ year, centred around the host season JAS(0) (see the three horizontal lines). The upper part of the correlation above the three lines represents precursory signals from the SST to the TOI(JAS), while the lower part represents precursory signals from the TOI(JAS) to the ENSO. It may be seen that the correlation values are appreciably larger when the TOI leads the ENSO (the positive time domain), from 0 to $+1$ year (see SL95).

This figure is obtained by applying the WAI for type II elimination to the result of Fig. 7 in Part I with a threshold $\varepsilon = 0.05$. Correlations are stronger with the removal of type II years, most notably they are larger when SST leads TOI (negative time domains, in the upper part of the diagram).

The host variable is next switched from the model variables to the observations. First the TOI(JAS) calculated for the model is replaced by the observed IMR(JAS). This further increases the correlations (Fig. 2), implying that the observed IMR(JAS) is indeed of good quality, and that it is more strongly correlated with SST than is the model's counterpart.

Based on the discussion in Part I, however, the observed TOI(JAS) may give even better results if an accurate observation set is available. The observed TOI(JAS) is calculated from the CRU data (see Table 1 of Part I). The result is shown in Fig. 3. Comparison with Fig. 2 indicates further improvement. Correlation magnitudes above

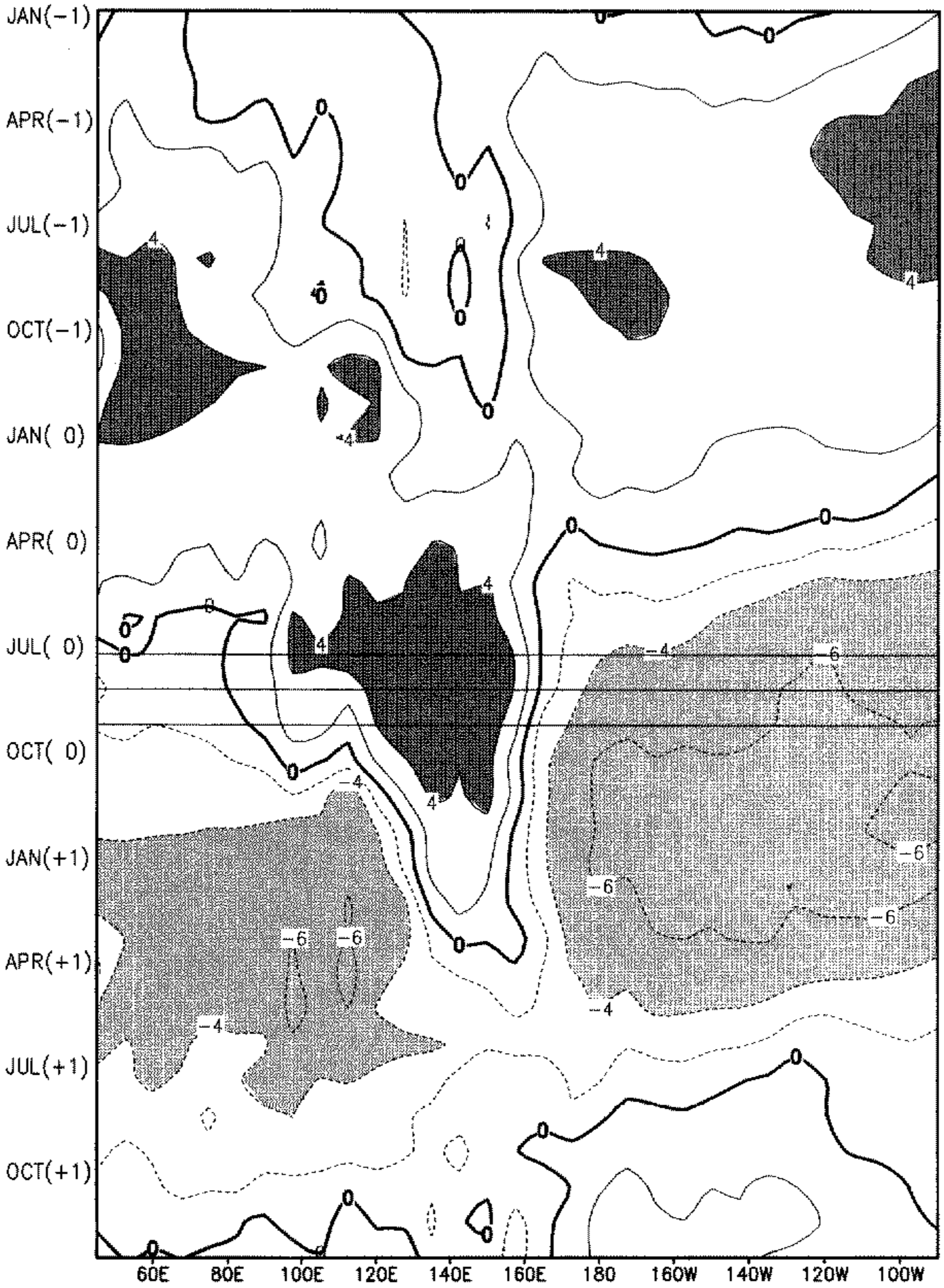

Figure 1. Longitude–time diagram of lag correlation (multiplied by 10), the model Tropical-wide Oscillation Index for July–August–September (TOI(JAS)), and the sea surface temperature anomalies over the 10°N–10°S belt along the Indo-Pacific longitudes. The ordinate is the lead or lag time from Jan(−1) (top) to Dec(+1) (bottom). The TOI(JAS) is referred to the middle of the ordinate, i.e. JAS(0) at which three lines are drawn. Contour interval is 2. The areas less than −4 are light shaded, and those greater than 4 are dark shaded. Type II years are eliminated (0.05 criterion).

0.8 prevail over large areas in Fig. 3. We argue that the type II separation has focused the analysis onto the ENSO–monsoon system appreciably.

According to Yasunari (1990) (hereafter Y90), the lag correlations between IMR and monthly averaged SST over the western and the eastern Pacific have maximum and minimum values in January(+1) and February(+1), respectively. Figures 1–3 agree approximately with this picture. As a whole, the periodic feature is emphasized by using

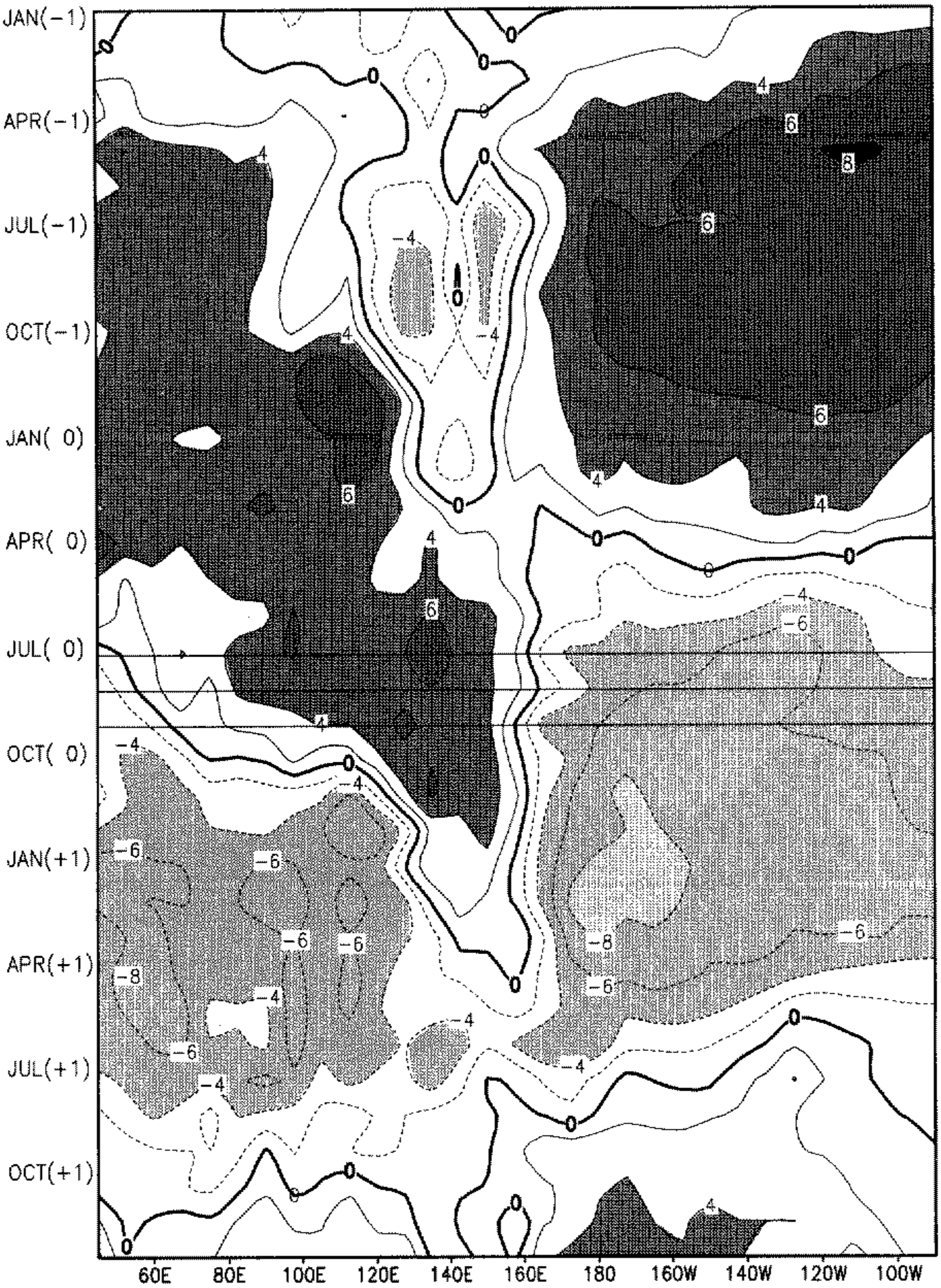

Figure 2. The same as Fig. 1, except that the host variable is the observed Indian monsoon rainfall for July–September.

better host indices and by applying type II separation. Note that the concept of a subset of years contributing more to ENSO–monsoon biennial linkages was put forth by Meehl (1987).

(*b*) *Vertical velocity lag correlation*

Similar diagrams to Figs. 1 and 2 but for omega at the 500 hPa level instead of SST were calculated. Here, only Fig. 4 is presented, in which the observed TOI(JAS) is the host and omegas of the three model runs are target variables, excluding the type II cases. Note that this diagram broadly resembles that with SST (Fig. 3). The correlation patterns

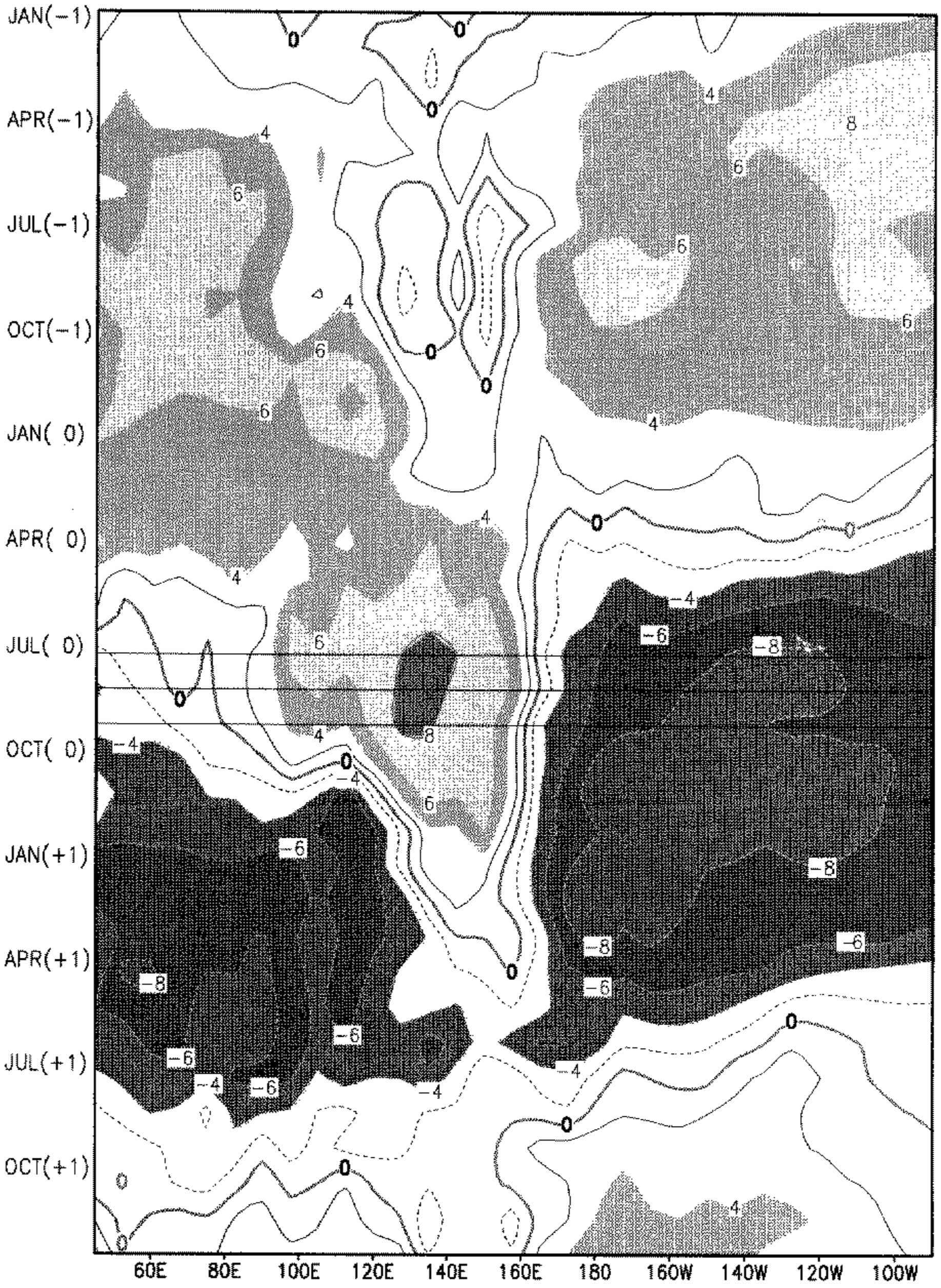

Figure 3. The same as Fig. 1, except that the host variable is the observed TOI(JAS) and the shading scheme is reversed.

of omega are continuously connected between the Indian and the Pacific sectors, and the correlation values are lower and less organized in the omega than in the SST maps.

A similar diagram, in which the host is the observed TOI(JAS) based on EOF 1 of the Xie–Arkin precipitation, and targets are the ERA omega, is calculated (not shown here). The result is encouraging; the overall pattern is very similar to Fig. 4, despite the extremely short time series of the ERA data. This suggests that the model anomalies are acceptable, at least, for the geographical distribution.

One of the interesting aspects in Figs. 1–4 is the fact that there is a large correlation value region in the middle, i.e. 110°E–160°E. This corresponds to the 'warm-pool'

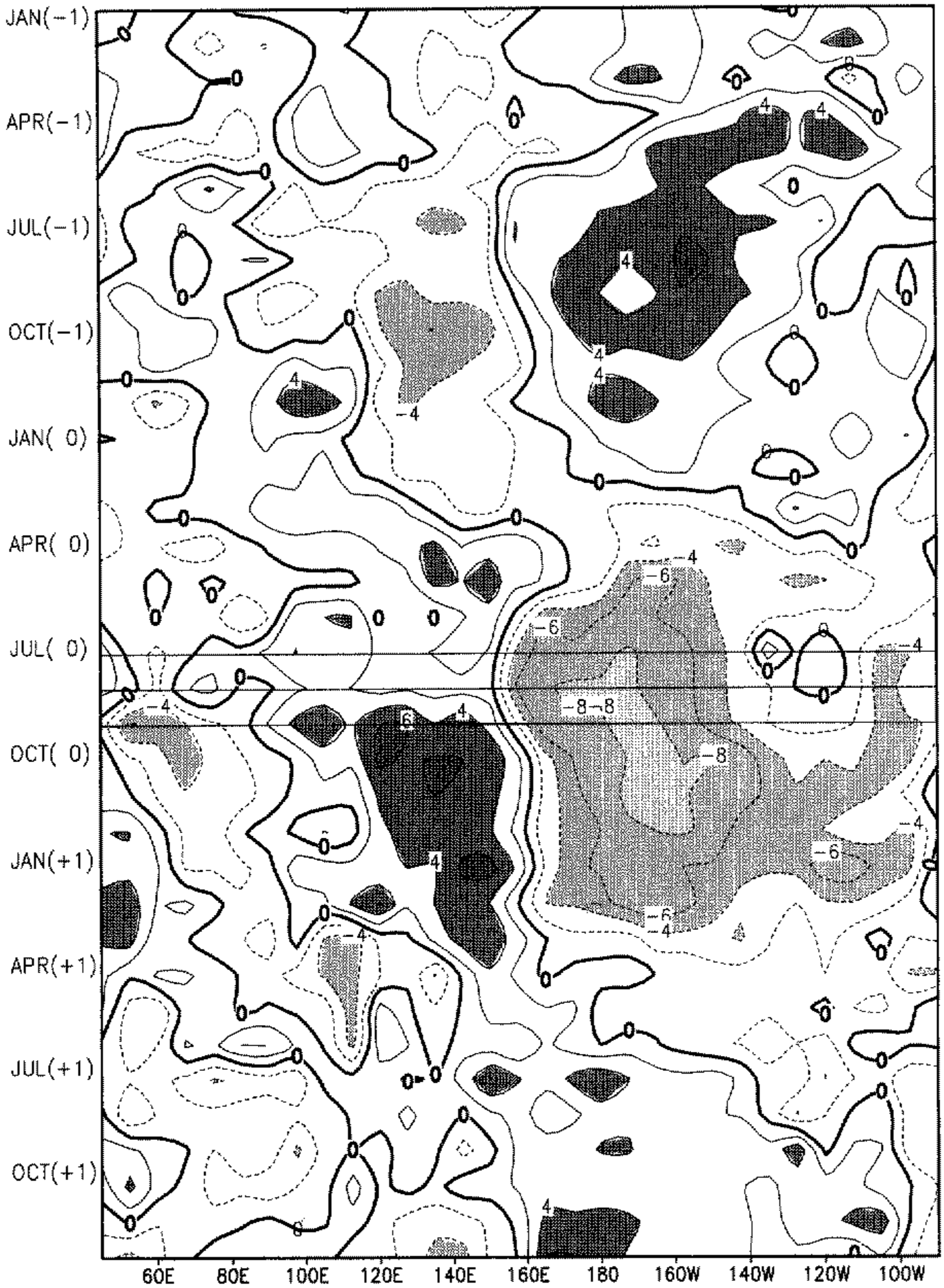

Figure 4. The same as Fig. 1, except that the target variable is the vertical velocity in the three model runs.

region at 5°S–15°N, which is located at the Timor Sea, the Mindanao Sea and the South China Sea. This appears a key area for the updraughts of the Walker circulation (see Figs. 10(a) and 10(b) of Part I), and is known as the 'doldrum' (Kutsuwada 1988). We also refer to this region in the next subsection as the 'Indonesian region'.

(*c*) *Host indices and type II elimination*

Tables 1 and 2 present summaries of the lag-correlation diagrams (like Figs. 1–3) for two target variables, i.e. SST (Table 1) and omega at the 500 hPa level (Table 2). There are five host variables (the first column), including the SOI; they are all for JAS. The

TABLE 1. MAXIMA AND MINIMA IN LAG-CORRELATION DIAGRAMS FOR SST OVER THE PACIFIC SECTORS, AND MAXIMA OVER THE INDONESIAN SECTOR

Host indices	Pacific minima		Pacific maxima		Indonesia	Cases
Model IMR	Feb(+1)	−0.35	Oct(−1)	0.05	0.20	I and II
	Feb(+1)	−0.57	Dec(−1)	0.43	0.45	I only
Model TOI	Nov(0)	−0.58	Oct(−1)	0.28	0.40	I and II
	Nov(0)	−0.65	May(−1)	0.50	0.53	I only
Obs IMR	Nov(0)	−0.71	Aug(−1)	0.43	0.48	I and II
	Mar(+1)	−0.88	May(−1)	0.81	0.70	I only
Obs TOI	Oct(0)	−0.88	Jun(−1)	0.47	0.67	I and II
	Nov(0)	−0.93	Apr(−1)	0.82	0.88	I only
Obs SOI	Oct(0)	−0.88	Mar(−1)	0.48	0.73	I and II
	Oct(0)	−0.93	Apr(−1)	0.63	0.81	I only

Left column specifies the host indices (see text); the second column includes times and correlation values for the minima; the third column includes those for the maxima; the fourth column is the maxima over the Indonesian sector; and the fifth column indicates the type II stratification.

TABLE 2. THE SAME AS TABLE 1 BUT FOR VERTICAL VELOCITY

Host indices	Pacific minima		Pacific maxima		Indonesia	Cases
Model IMR	Mar(+1)	−0.38	Oct(−1)	0.20	0.38	I and II
	Feb(+1)	−0.43	Nov(−1)	0.40	0.50	I only
Model TOI	Dec(0)	−0.43	Oct(−1)	0.27	0.40	I and II
	Dec(0)	−0.53	Oct(−1)	0.40	0.55	I only
Obs IMR	Oct(0)	−0.53	Oct(−1)	0.41	0.43	I and II
	Oct(0)	−0.72	Jul(−1)	0.63	0.52	I only
Obs TOI	Oct(0)	−0.72	May(−1)	0.40	0.53	I and II
	Oct(0)	−0.83	Aug(−1)	0.62	0.63	I only
Obs SOI	Dec(0)	−0.73	Jul(−1)	0.27	0.45	I and II
	Dec(0)	−0.80	Jul(−1)	0.45	0.61	I only

observed host indices (except the SOI) are calculated based on the CRU precipitation data.

The Tables show the minimum and maximum values of the correlation over the central and the eastern Pacific (160°E–80°W) and the maximum value in the Indonesian sector (100°E–160°E). Let us take an example of a host index, the observed TOI in the first column. The values in the Table are based on Fig. 3. There are two sub-rows within a row of the table. The upper sub-row indicates that, over the eastern Pacific, the minimum occurs in Oct(0) with a correlation of −0.88 and the maximum occurs in Jun(−1) with 0.47; and the Indonesian maximum is 0.67. On the other hand, the lower sub-row, based on Type II separation, indicates that the minimum occurs at the month of Nov(0) with a correlation of −0.93, while the maximum occurs in Apr(−1) with 0.82 correlation (substantially improved and occurring in a different month from above); and the Indonesian maximum is 0.88 (also improved).

The bottom rows of Tables 1 and 2 are the correlations using the SOI as the host variable (using Fig. 5). It is evident that the SOI has somewhat lower correlation in the negative time domain, compared with the TOI in Fig. 3.

The contents of these tables may be summarized as follows.

(1) The TOI gives stronger correlation than the IMR consistently.

(2) The observed TOI gives better correlation than the observed SOI, considerably so in the negative time domain with type II removed.

(3) Removal of type II years improves correlation values without exception. The increase is particularly large in the negative time domain; the largest increase was 0.38

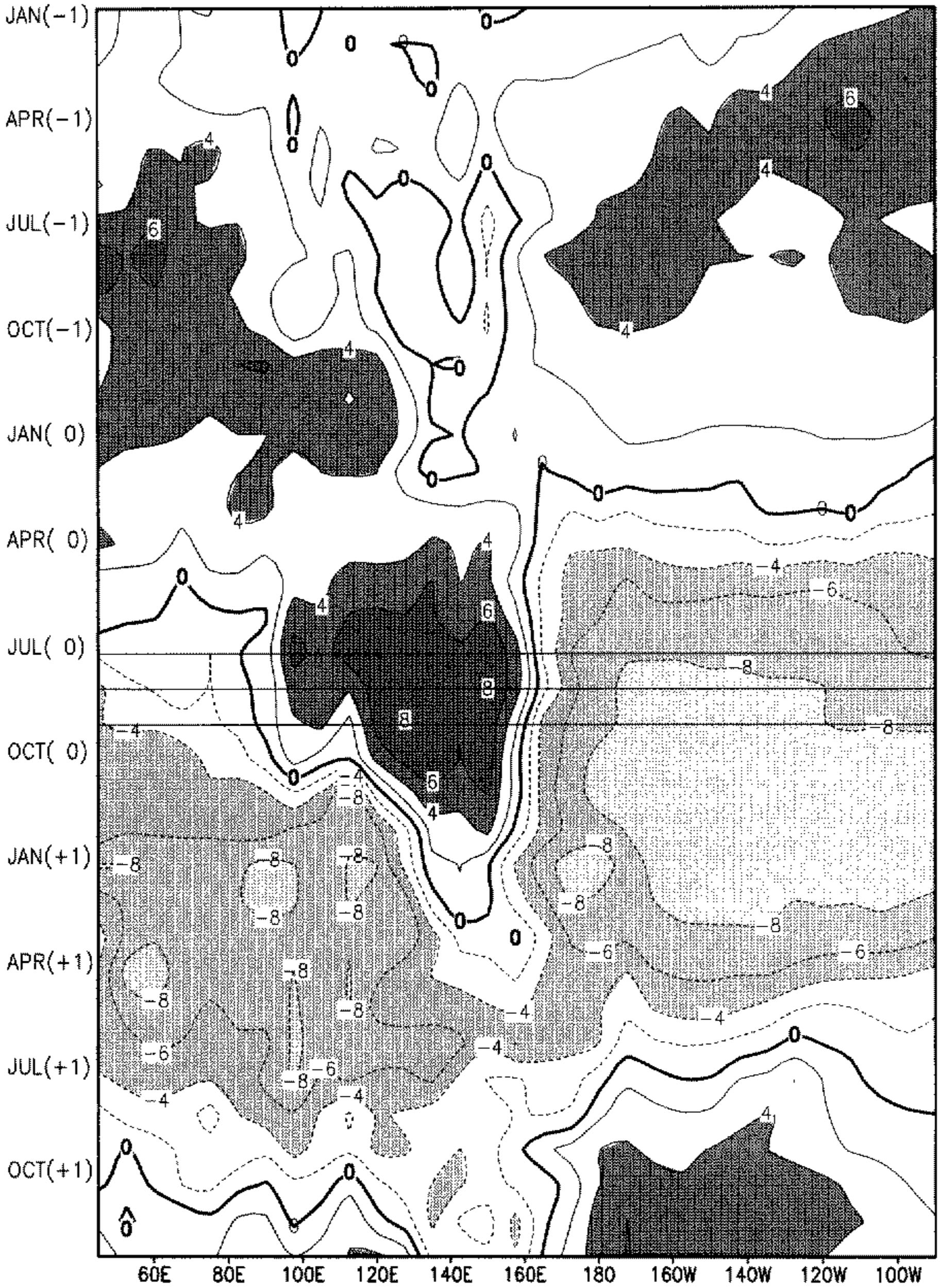

Figure 5. The same as Fig. 1, except that the host index is the observed Southern Oscillation Index for July–September.

in Table 1, for the model as well as observed IMR, i.e. the first and third rows. Part of the reason is that the sample number is decreased in the negative time domain due to type II elimination for two successive years. The significance levels in the negative time domain are: 80.00% (correlation, corr = 0.20), 95.00% (corr = 0.40) and 99.00% (corr = 0.47) in type I and II, while 90.00% (corr = 0.40), 95.00% (corr = 0.50) and 99.90% (corr = 0.81) in type I only.

The minima appear between Oct(0) and Apr(+1), i.e. 3 ~ 7 months after JAS(0). This period often covers the peak of the El Niño, i.e. Nov(0)–Dec(0)–Jan(+1), and the peak of La Niña, i.e. Aug(0)–Sep(0)–Oct(0) (Shukla, personal communication).

Based on this evidence, November–December–January (NDJ(+1)) is taken approximately as one of the peak phases of the system, a point which will be utilized in the analysis of the next subsection. Similarly, the maxima appear between Feb(−1) and Oct(−1), i.e. ~10–17 months before JAS(0). The period is spread widely, but in part corresponds to the peak of the Asian monsoons in boreal summer. Based on this fact, 'JJA(−1)' is taken approximately as another peak phase of the ENSO–monsoon system.

The TOI and the SOI perform best for the positive domain, while the TOI and IMR perform best for the negative domain and hence the biennial characteristic. In this sense, the SOI is more associated with the ENSO than the Asian monsoons, whereas the TOI(JAS) embraces the ENSO and the monsoons more equally.

(*d*) *Vindication of the two indices*

Utilization of indices derived from a principal component analysis (or EOF analysis) of meteorological variables was attempted in the 1960s and 1970s by a number of investigators, such as Kutzbach (1967), Kidson (1975), Wright (1975), and Trenberth (1976), using data at several widely spread stations. In variables employed by Walker and Bliss (1932), the index was derived so as to have a high correlation with the contributing stations; hints were given at the derivation of EOF 1. Recently, Thacker and Lewandowicz (1996) advocated the general principle of indices; any efficient index should characterize the chosen field with as much detail and accuracy as possible.

Further evidence on the utility of EOF 1 has been presented here; the TOI(JAS) appears superior to the IMR(JAS) or the SOI(JAS) as an index that links the tropical rainfall for JAS with omega or SST in the tropics. We have not investigated all possible indices; for example, the Webster–Yang index. This index is used extensively by Ju and Slingo (1995) in their study of the Asian summer monsoon and the ENSO.

As Soman and Slingo (1997) commented, an index should be robust and easily and accurately obtainable. To investigate the robustness of our index, the TOI(JAS) was recalculated using the Xie–Arkin data. As shown in section 7 of Part I, the agreement with another calculation based on CRU data is satisfactory.

It has been demonstrated so far that exclusion of type II cases always enhances the correlation in all Tables and diagrams. Yet it is still possible that the notion of strong/weak SST signal alone is sufficient for identification of a good/poor ENSO–monsoon system, the idea being raised as a counter argument against the method of type I/type II separation (see Part I and subsection 2(b)).

To address this criticism, we have examined the following.

(i) Has the elimination of some cases contributed to the inflated correlation?
(ii) Would the elimination of years characterized by 'weak SST' yield similar correlation to, or stronger correlation than, the elimination of type II years?

It is a statistical fact that if 'near normal' cases are removed from two normally distributed time series with a certain cross-correlation, then the cross-correlation will on average be increased. While the type II separation is not performed so as to directly focus on the ENSO–monsoon extremes, in practice there is a tendency for this, and the worst-case scenario would be for the improvements reported to be solely attributable to statistical artifact. To check that the increases in cross-correlation in Tables 1 and 2 are above that expected from focusing on extremes, 500 pairs of time series (x, y) of

length 34 were generated with a mean cross-correlation of 0.35. Then, the 15 smallest-amplitude cases were deleted from each of the 500 x-series, and the correlations recalculated using the 500 pairs, now of length 19 (the number of cases retained matches the number of years available to construct the type II removed correlations in Tables 1 and 2—recall that two consecutive years must be type I in order to contribute to the lagged correlations). In the Monte Carlo experiment, the 500 correlations were, on average, increased by 0.1 by focusing on extremes. The 5% significance point was an inflation of 0.22 (i.e. 25 out of 500 correlations were inflated by more than 0.22) and no correlation was inflated by more than 0.33. It seems clear that the increase in correlation in the negative time domain in Tables 1 and 2 is well above that expected merely from focusing on extremes. It is noted, however, that the positive domain is not confirmed; we shall come back to this point later.

Concerning the second criticism, we made an additional experiment, using a different classification of strong/weak teleconnection. According to Table 1 in Part I, 'EST' gives the normalized SST(JAS) in the eastern equatorial Pacific. The cases of strong/weak signals of SST anomalies can be specified based on the value of EST. By using the threshold value $\varepsilon = 0.25$, the 'weak years' are chosen as: 1961, '68, '78, '79, '80, '83, '92 and '93. These years are removed in order to make the same sample numbers, and comparison is made on the effectiveness for identifying teleconnection by using both methods. The results are summarized as follows.

The correlation for the case of the observed TOI (Table 1 4th row and the column of maxima) is worse by the 'weak SST' method (former) than by the WAI method (latter); the correlation is 0.73 in the former, as opposed to 0.82 in the latter. A decrease in correlation is more noticeable in the Indian sector in the former than in the latter. In fact the correlation is even worse in the former than by doing nothing. This may imply that the type I years are important and crucial over the Indian sector, as was speculated in section 6(a) of Part I. Thus, it is concluded that type I/type II separation based on the WAI is more effective than the elimination of the weak SST method.

4. The ENSO–monsoon system as a biennial oscillation

(a) *Teleconnection maps*

As seen in Figs. 1 and 4 and Tables 1 and 2, lag correlations between the TOI(JAS) and the SST or omega are large over much of the equatorial Indo-Pacific. In order to expand the view of the teleconnection beyond the equatorial region, a global map analysis of lag correlation is performed, following Y90.

Figures 6 to 9 present these maps. The host index is the observed TOI(JAS), while the target variables are the model's omega in Fig. 6, the Xie–Arkin precipitation in Fig. 7, the SST in Fig. 8 and the model's sea-level pressure (SLP) of the atmosphere in Fig. 9. The results of the ECHAM4 model in Figs. 6 and 9 compare reasonably with the observations (not shown). The top panels of the four Figures are the lag correlations of target variables for JJA(−1), the middle panels are the almost simultaneous correlations, because they use JAS(0) for TOI and JJA(0) for the target variable, and the bottom panels are lead correlations for November–December–January, NDJ(+1). They are the geographic representations of the time–longitude plots shown earlier. Namely Fig. 4 corresponds to Fig. 6, and Fig. 3 corresponds to Fig. 8. The type II years are removed from all maps with threshold $\varepsilon = 0.05$, except $\varepsilon = 0.03$ for Fig. 7, because of the smaller sample size. The simultaneous correlation maps have been referred to as 'teleconnection' maps (Sperber and Palmer 1997).

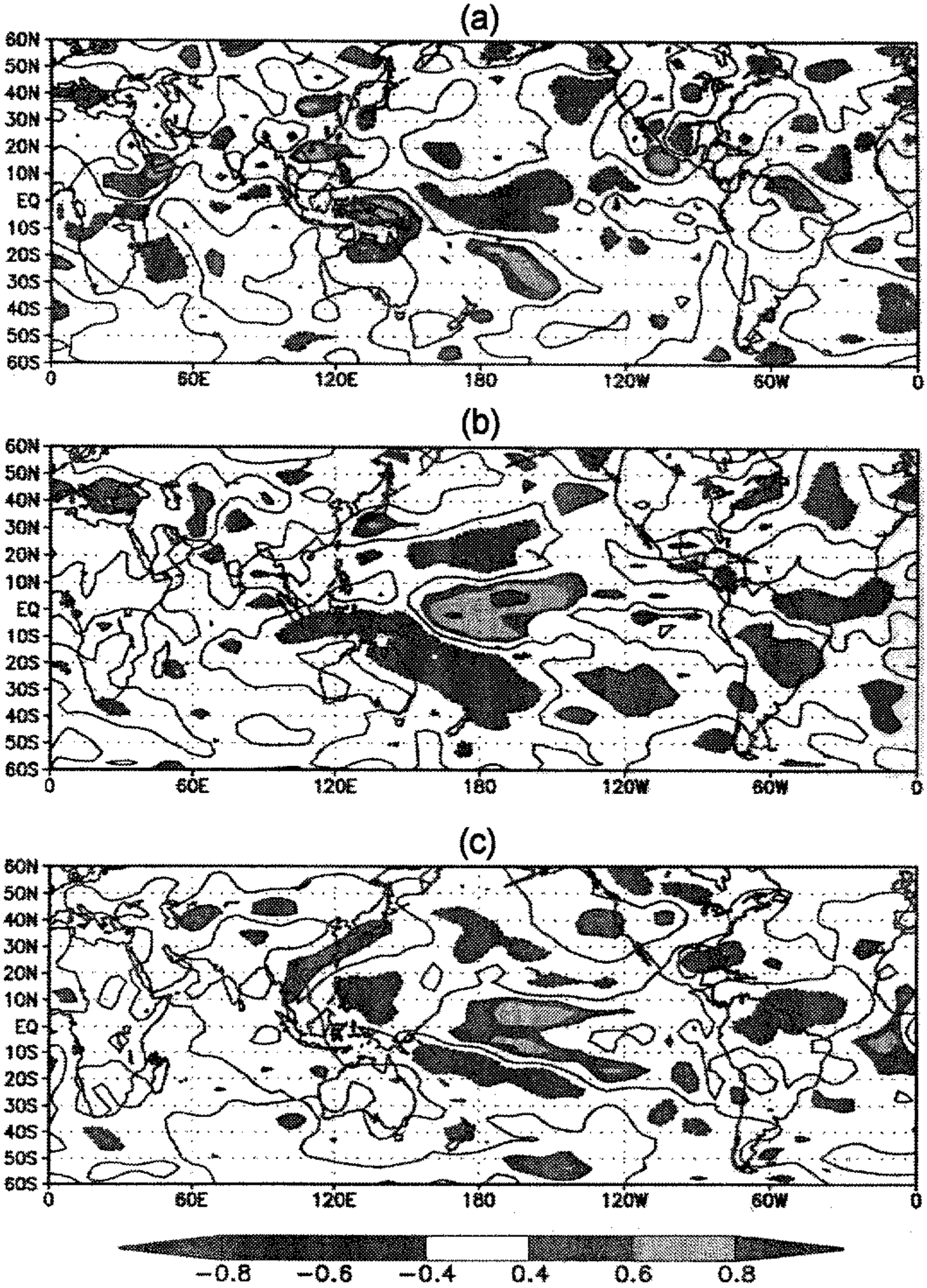

Figure 6. Teleconnection maps, i.e. geographical distribution of lag correlations. Host index is the observed Tropical-wide Oscillation Index for July–August–September (TOI(JAS)), and target variables are the model vertical velocity of three runs; (a) for June–July–August(−1); (b) for June–July–August(0), and (c) for November–December–January(+1). Contour interval is 0.2.

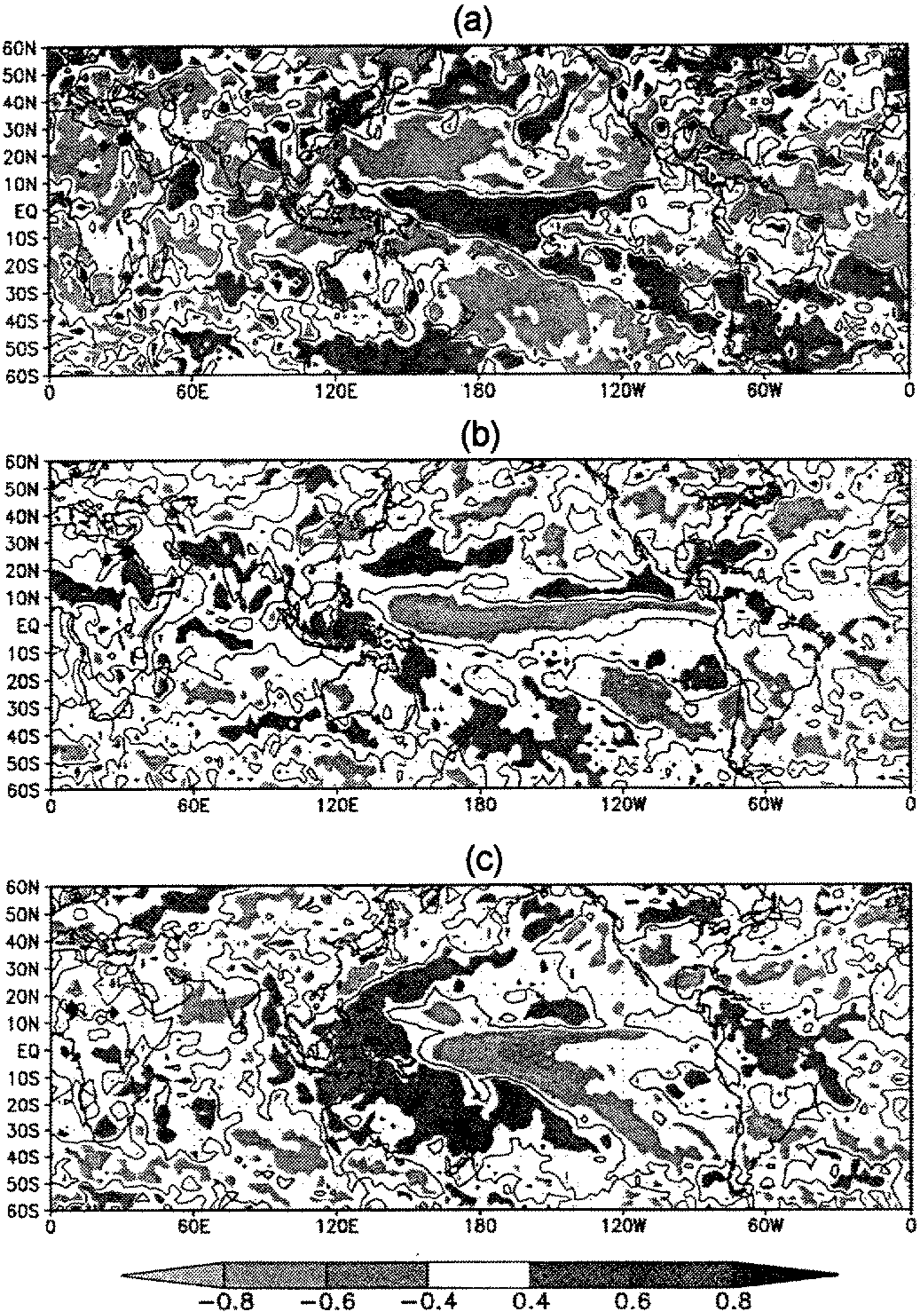

Figure 7. The same as Fig. 6, but the correlation between the observed TOI(JAS) and the Xie–Arkin precipitation.

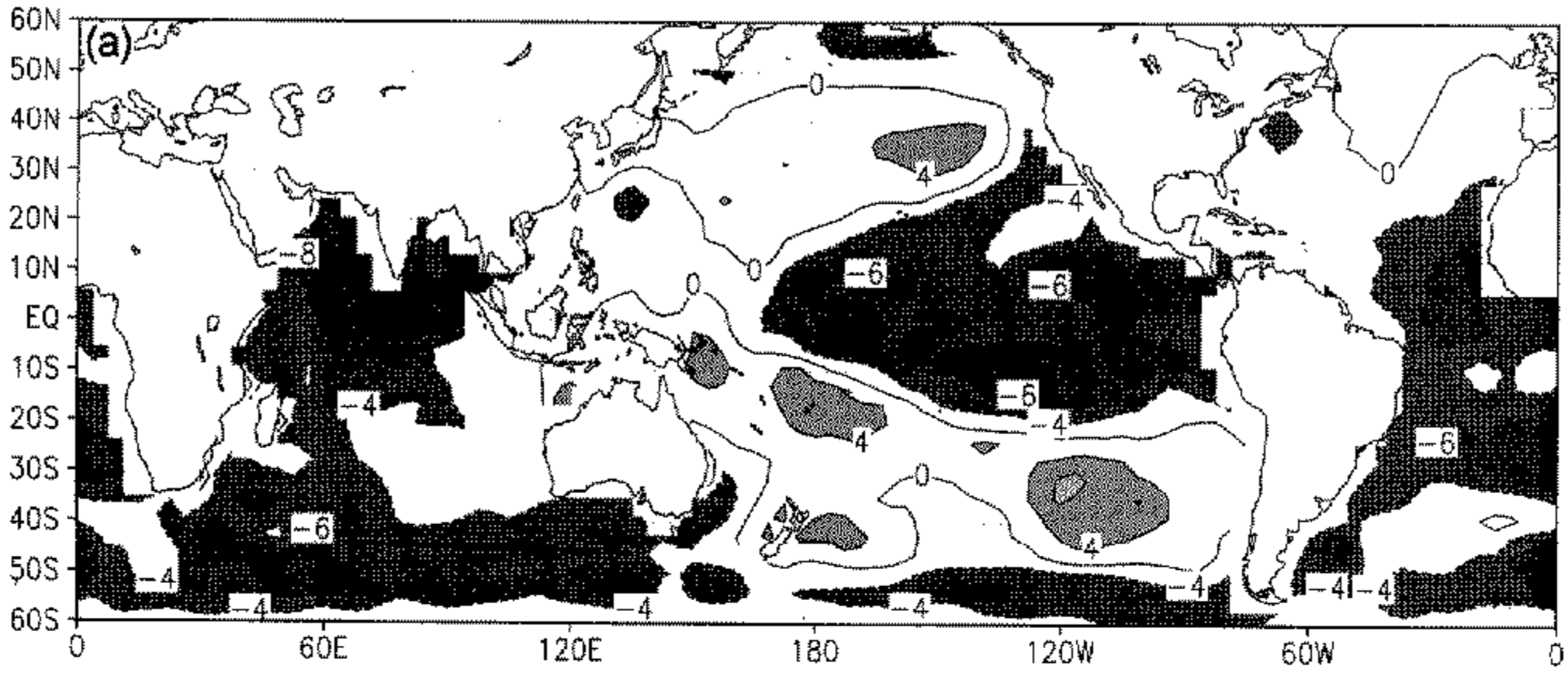

Figure 8. The same as Fig. 6, but the correlation (×10) between the observed TOI(JAS) and the sea surface temperature.

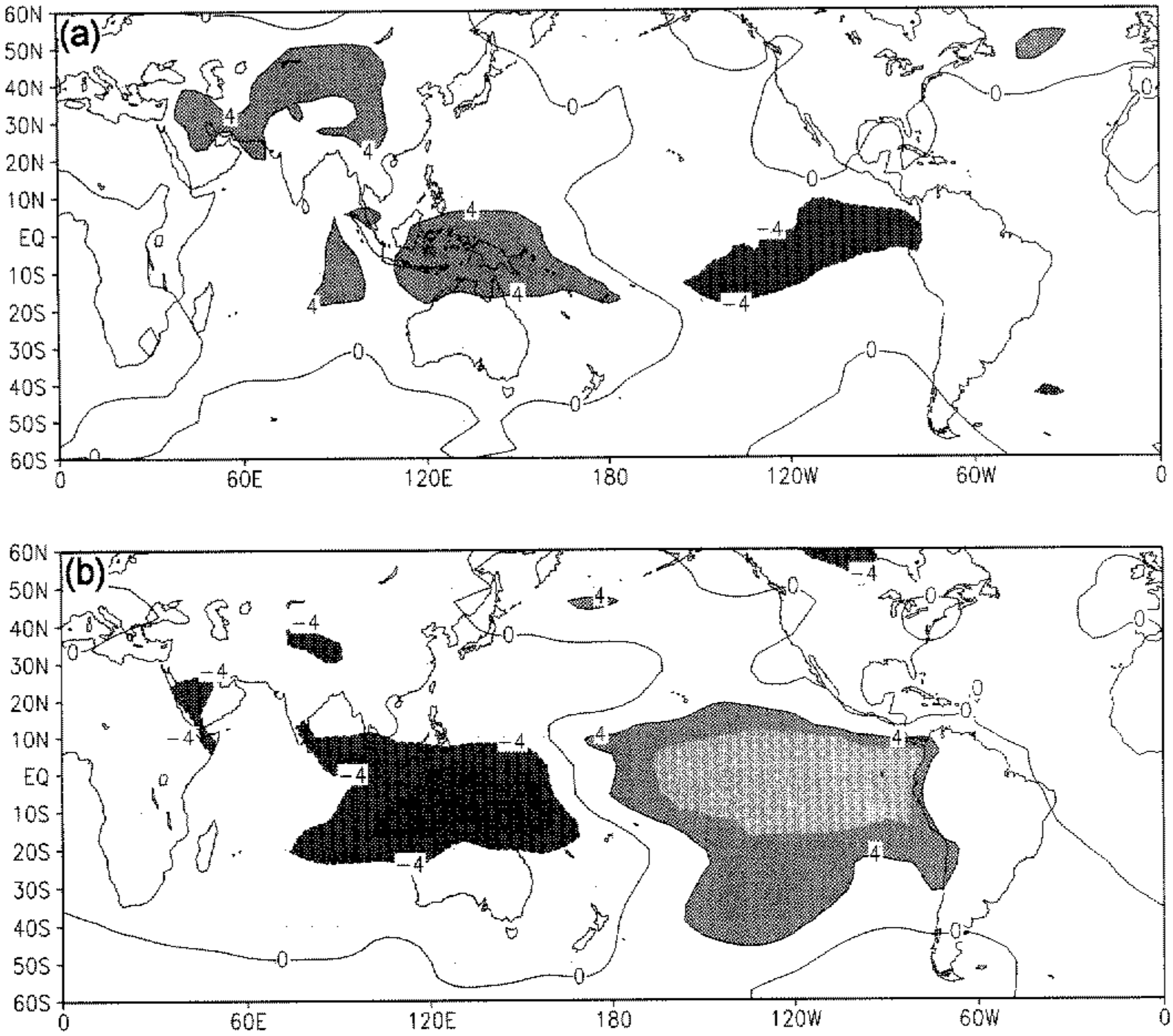

Figure 9. The same as Fig. 6, but the correlation (×10) between the observed TOI(JAS) and the model's sea-level pressure.

All patterns in the top and middle panels have opposite signs, showing a biennial oscillation. Since these diagrams are for correlation, the intensity of target variables is proportional to that of the TOI(JAS(0)). It is interesting to note that the oscillation of the Indian Ocean SST (Fig. 8) is quite different from that of the Pacific Ocean. Most oscillations are standing, though an exception is the region along the coast of China (e.g. see Fig. 6). Another interesting point is that the correlation values at the 13-month lag (top panels) are not negligible, particularly in Figs. 8 and 9, and they also show that the effect of the ENSO–monsoon oscillation spreads to the extratropics and the Atlantic Ocean. At NDJ(+1) (bottom panel) high correlation values are found over both hemispheres, reflecting that NDJ(+1) includes peaks of the El Niño in boreal winter. It is of particular importance to note that there is no peak at NDJ(0) over the Pacific sector (see Fig. 3). Figure 3 and Tables 1 and 2 show that the season JJA(−1) (top panels, Figs. 6–9) is the other peak of opposite sign to that for NDJ(+1). The analysis here allows us to describe a biennial oscillation in the ENSO–monsoon system from boreal summer of −1 year to the following summer of 0 year, followed by intensification of the El Niño to NDJ(+1). The last point seems to preclude a return to opposite ENSO–monsoon biennial phase in boreal summer(+1) (see Fig. 3). Thus, the ENSO–monsoon oscillation system is not sinusoidal but skewed. It is intriguing, and the consequence deserves further study.

Another interesting aspect is that, at least, two types of patterns are identified, i.e. the horseshoe (Figs. 6 to 8) and the see-saw (Fig. 9), which will now be described.

(*b*) *ENSO–monsoon oscillation patterns*

The horseshoe patterns are largely symmetric around the equator over the Pacific; this is particularly so for the SST (Fig. 8). These horseshoes are surrounded by one or two outer rims on the western periphery. The first rim goes through the Indonesian sector (the warm pool), including the South Pacific Convergence Zone (SPCZ)-like band and the northern hemispheric counterpart (referred to as the NPCZ in Part I). The second rim goes through the coast of China, though this band can be seen only in NDJ(+1) (bottom panels of Figs. 6–8). These features agree well with those of Y90. Concerning the teleconnection maps of omega and precipitation (Figs. 6 and 7), the presence of the Inter-Tropical Convergence Zone (ITCZ) over the North Pacific, and SPCZ over the South Pacific modify the equatorial symmetry significantly.

The eastern hemisphere, i.e. the Asian monsoon area, is occupied by the rim of the horseshoes. The configurations of teleconnection are affected by the presence of the continent and, therefore, they deviate from the north–south symmetry, particularly for precipitation and omega. This is exactly the reason for the utility of TOI(JAS), as opposed to TOI(JFM). In JJA(−1), the western rims of the Pacific horseshoe are open through the Philippine Island area, and the Pacific and the Indian sectors are connected with each other. The eastward tails of the horseshoe in NDJ(+1) extend nearly to the west coast of the USA in omega, and to the south-east of USA in precipitation, and the influence is seen even as far as north-eastern South America and Argentina (see Rasmusson *et al.* (1981) and Ropelewski and Halpert (1989)).

As described earlier, the horseshoe distribution is characteristic of the variables, SST, omega, and precipitation. On the other hand, Fig. 9 presents maps of the SLP, which forms the see-saw pattern. The procedure for deriving this map is exactly the same as that for Figs. 6 and 8. Van Loon and Shea (1985, 1987), Trenberth and Shea (1987), Kiladis and Van Loon (1988), Kiladis and Diaz (1989), and Ju and Slingo (1995) described the standing oscillation or see-saw patterns by computing lagged correlations for SLP between Darwin and other selected locations. The centres of opposite signs

are located over Indonesia and the central South Pacific Ocean, and the key feature is 'the SPCZ which approximates the dividing line between the two centres of action' (Trenberth and Shea 1987). Figure 9 looks slightly different from this description, but is essentially the same (see also Wright (1985)).

The horseshoe pattern, such as the SST correlation map for JJA(0) (Fig. 8(b)), has been found in various previous investigations, e.g. the SST map in the 'mature phase' of the El Niño (Rasmusson and Carpenter 1982), the EOF 1 of the global SST (Hsiung and Newell 1983), and others. Wright (1985) also presented this pattern as the correlation maps between the annual mean SLP at Darwin and the annual mean values of precipitation, or air temperature. Wright's patterns are symmetric around the equator, though the peripheral rims are opened at the Z-region, in the same way as in the patterns for JJA(−1) in Figs. 6 and 8. The horseshoe pattern can also be obtained by applying a quasi-biennial band-pass filter to the SST anomalies (e.g. Barnett 1991; Tomita and Yasunari 1996, Fig. 1). Figure 8(c) (NDJ(+1)) resembles most of the ENSO mode of Penland and Sardeshmukh (1995) (pattern 'b' of their Fig. 2), and the December–January–February (DJF) composite map of SST anomalies for the biennial oscillation type (Ose *et al.* 1997).

(*c*) *Periodicities*

The biennial or quasi-biennial periodicity is a unique and important characteristic of the ENSO–monsoon system, as has been pointed out by, for example, Trenberth (1975), Nicholls (1978), Trenberth and Paolino (1981), Rasmusson and Carpenter (1982), Barnett (1983, 1991), Bhalme and Jadhav (1984), Van Loon and Shea (1985), Gutzler and Harrison (1987), Meehl (1987, 1994), Lau and Sheu (1988), Kutswada (1988), Rasmusson *et al.* (1990), Mooley and Munot (1993), Annamalai (1995), and Terray (1995).

Jiang *et al.* (1995) investigated 40-year time series of SST and surface zonal wind over the equatorial Pacific, using the technique of multiple singular spectral analysis, and obtained three major peaks in the spectrum of the two combined variables. The first peak is the 12-month cycle; the second is the 53-month cycle, which is denoted by the QQ (quasi-quadrennial) mode; and the third is the 28-month cycle, denoted by the QB (quasi-biennial) mode. The QQ mode is the most dominant component for the ENSO phenomena, and it contributes 28.5% of the NINO3 SST variance, while the QB mode contributes 18.4% of the variance. Penland and Sardeshmukh (1995) applied the empirical normal mode technique to the 41-year time series of observed SST data over the tropical Indo-Pacific basin, and obtained the 46 and 25-month periodicities, as the ENSO related modes, which are almost the same as ours.

It is a puzzle why the TOI(JAS) can work so well (high correlation) in this paper for constructing lag-correlation diagrams and lag-teleconnection maps, and also why Penland and Sardeshmukh (1995) obtained the correlation of as much as 0.87 between the composite time series of SST and the observation, and derived the periodicities close to 48 and 24 months. The reason may be that the peaks of the QQ mode are seasonally locked; the SST anomalies in the major El Niño are largest for NDJ; and, besides, this mode appears to be cooperatively involved in the biennial diagrams and maps. Namely, the correlations over the Pacific sector are not strong at NDJ(0), but are strong at NDJ(+1). Perhaps this is because the correlation view emphasizes bursts of regular behaviour, whereas the spectral view emphasizes 'best-fit' regular behaviour throughout. Yet in the case of Penland and Sardeshmukh, the cosine/sine modes with three periodicities, 46, 25 and 72 months, are used and show good agreement of time series of SST between the observed and the three-mode synthesis. It is, then, an

interesting and crucial question whether the QB mode is indeed reduced to a biennial mode by the type II elimination, as was first noted by Meehl (1987) as the Tropospheric Biennial Oscillation (TBO).

Ropelewski *et al.* (1992) show the Hövmoller diagram (their Fig. 9) of the surface zonal wind anomaly as well as the SST anomaly over the equatorial Indo-Pacific longitudes. The biennial periodicity of the wind anomalies over the western Pacific is distinct in their diagram. Different from the quasi-biennial oscillation in the stratosphere, the durations of oscillation coincide exactly with a multiple of 12 months. Namely, the phase of QQ and QB are precisely locked to the annual cycle. Two-year oscillations emerge not suddenly; they continue for three or four successive years, and disappear not suddenly either. If one plots type II years (shown in Table 1 of Part I) in the Ropelewski *et al.* diagram, they almost fit; three out of four type II years agree with each other. Yet it should be noted that the El Niño and La Niña are not symmetrical in terms of the timing of SST anomaly occurrence and, in that sense, the ENSO is a skewed oscillation.

When revising this paper, two papers came to our attention, i.e. Tomita and Yasunari (1993) and Ose *et al.* (1997). They proposed an idea about two types of ENSO, i.e. BO-type (biennial oscillation) and LF-type (low frequency). Depending on the type, the tropical eastern Pacific SST anomalies change in the following spring (BO) or are maintained for two or more years (LF). This classification is quite different from type I and type II, except that one of the two years in the LF type coincides with a type II year for all cases of LF. This point needs further investigation.

Returning to Figs. 6–9, the patterns look simple and regular. A part of the reason is that these patterns are statistical representations, but the main reason is that the monsoons are biennial phenomena, and the ENSO is a kind of quadrennial monsoon (seasonal fit—Philander (1990), for example). Therefore, the contents involved in these figures are quite rich, due to the information included in the TOI(JAS). Some practical implications will be shown by forecast experiments in the next section.

5. Empirical forecasts and biennial oscillation

(*a*) *Fifteen-month forecasts of the IMR(JAS) from the Pacific SST*

Another way to visualize the correlation pattern in Fig. 8 is to separate the SST distributions into two groups, depending upon the signs of the time coefficients of the TOI(JAS(0)). For example, take the correlation value at a point in the longitudinal–time diagram (for example, Fig. 1), i.e. Jul(0)–140°W, which is −0.50. Analysis reveals that the negative sign occurs in 19 of the total 34 years of data; the rest contributes to the correlation reversely. Among the 19 contributing years, 8 cases contribute to the correlation for wet monsoons, while 11 cases contribute to that of dry monsoons. Thus two composite SST maps are generated for wet/dry monsoon anomalies, based on 8 and 11 cases (years). Before wet monsoon cases, positive SST anomalies up to +3.0 degC appear, while before dry monsoon cases negative anomalies, −2.4 degC, appear (not shown). This result is consistent with Verma (1994), and it is quite similar to Ju and Slingo (1995). It is noted again, however, that the positive and negative anomalies are not exactly symmetrical around the zero line with respect to magnitude and timing. Both for rainfall and SST, the positive anomalies tend to occur later in time and larger in magnitude.

As the second implication of the teleconnection maps, we produce experimental forecasts. In Fig. 3 and Fig. 2, there are positive peaks at Apr(−1) and May(−1) over the eastern Pacific (correlations of 0.82 and 0.81, respectively). Thus the SST over the Pacific 15 or 16 months before JAS(0) is closely related with the TOI(JAS(0)) or the

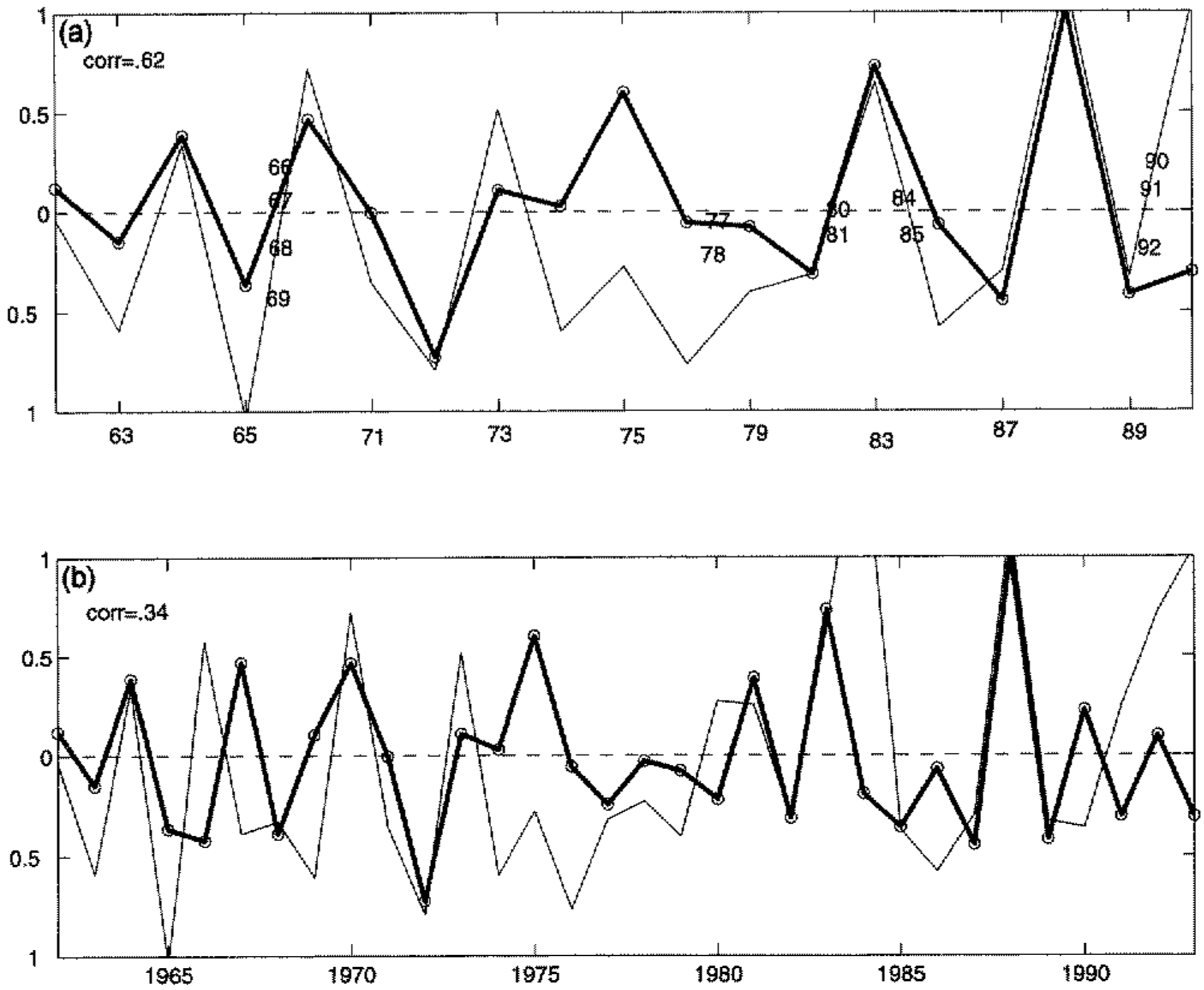

Figure 10. Fifteen-month projection of Indian monsoon rainfall (IMR) (i.e. JAS(0)) from the sea surface temperature (SST) (May(−1)) over the eastern equatorial Pacific. The thick solid line is the normalized IMR (the predictand) and the thin solid line is the normalized SST (the predictor). (b) The verification of all years, and (a) the verification for the remaining 19 years after the year(−1)/year(0) type II elimination. Included predictand years are labelled at the bottom of (a). The eliminated predictand years (year(−1) or year(0) was type II) are indicated near the central dashed line of (a).

IMR(JAS(0)). This suggests that a 15 or 16-month projection of the TOI or IMR may be possible by using the information of the SST over the eastern Pacific. Figure 10 shows experimental forecasts of IMR, based on the SST over the eastern Pacific (120°W–100°W, 10°N–10°S) (we simply plot the two indices together for this demonstration—a regression forecast relationship would re-scale the SST optimally in a least-squares sense, but make no difference to the correlation skill). The correlation skill for the IMR forecasts is 0.34 and 0.62 including and excluding type II years, respectively, while the correlation skill for TOI forecasts is 0.41 and 0.77 (not shown). It should be noted that the forecasts in Fig. 10(a) require advance knowledge in May(−1) that JAS(−1) and JAS(0) will be type I (since this criterion must be satisfied for inclusion in the analysis). To be of practical use, therefore, methods of forecasting type I or type II states are needed, perhaps using coupled ocean–atmosphere models or using the three-dimensional state of the tropical Indo-Pacific Ocean in May(−1). For a purely empirical approach to this problem, inspection of Table 3 of Part I shows that if JAS(−2) is type II, and JAS(−1) is type I, then a forecast of a transition into opposite phase TOI and IMR for JAS(0) shows good promise (100% sign skill for the IMR and TOI anomaly in the seven forecasts, including four extreme TOI and IMR events). Detailed development of an operational forecasting method is beyond the scope of this paper; however, we wanted

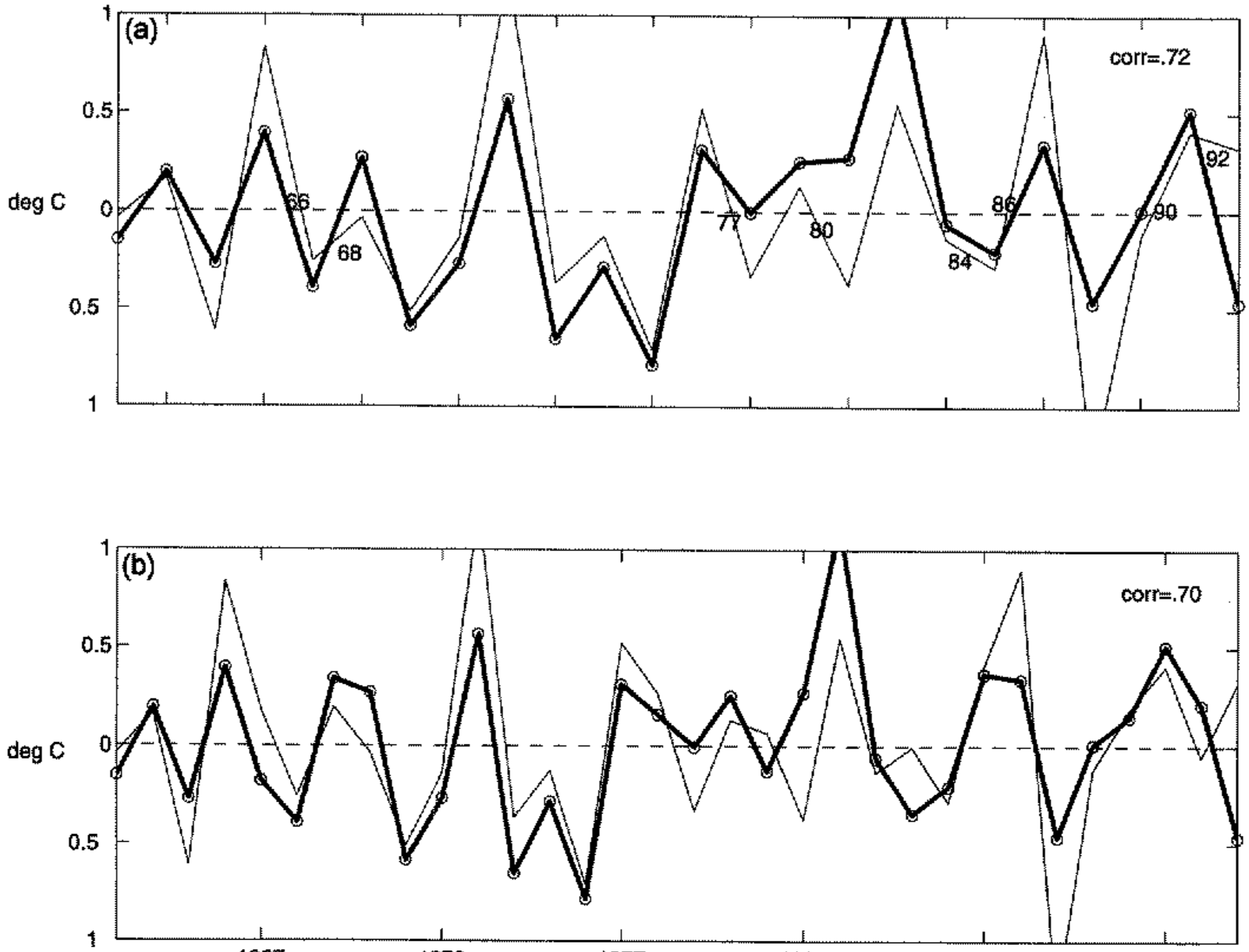

Figure 11. Same as Fig. 10, but for a four-month projection of NINO3 sea surface temperature (i.e. January(+1)) from the observed Tropical-wide Oscillation Index for July–August–September. (a) Verifies the remaining 24 years after type II elimination (here, years are eliminated if year(0) is type II). The type II years are marked near the central dashed line of (a).

to suggest the ways in which the type I/type II concept might be used for practical forecasting in the future.

If one tries to forecast the IMR of TOI with a shorter lead-time, say 4 to 7-month forecasts (as Walker (1936) tried for IMR), the results are not good using the SST over the Pacific (not shown), even when type II years are eliminated.

(*b*) *Four-month forecasts of Pacific SST and US precipitation from TOI(JAS)*

Figure 3 and Table 2 suggest that the lag correlation between the TOI(JAS) and SST anomalies at Jan(+1) is −0.93. This means that a 4-month projection of the SST at the central and eastern Pacific can be made by using the information of TOI(JAS). Figure 11 is the result of an attempt at a 4-month forecast (Jan(+1)) of SST anomalies over the NINO-3 region (150°–90°W) using the TOI(JAS(0)) as the predictor. Figure 11(b) is the verification including all years (correlation is 0.70), and these forecasts are improved slightly by eliminating type II years, as is shown in Fig. 11(a) (correlation is 0.72). The TOI for JAS(0) is the predictor, while the target predictand (the SST) is for the following year Jan(+1). The type II elimination is based on WAI for year(0). For example, if the year 1966 is of type II, the SST for 1967 is eliminated. In fact, the improvement in the forecast skill with type II separation is here only small. We will come back to this problem later.

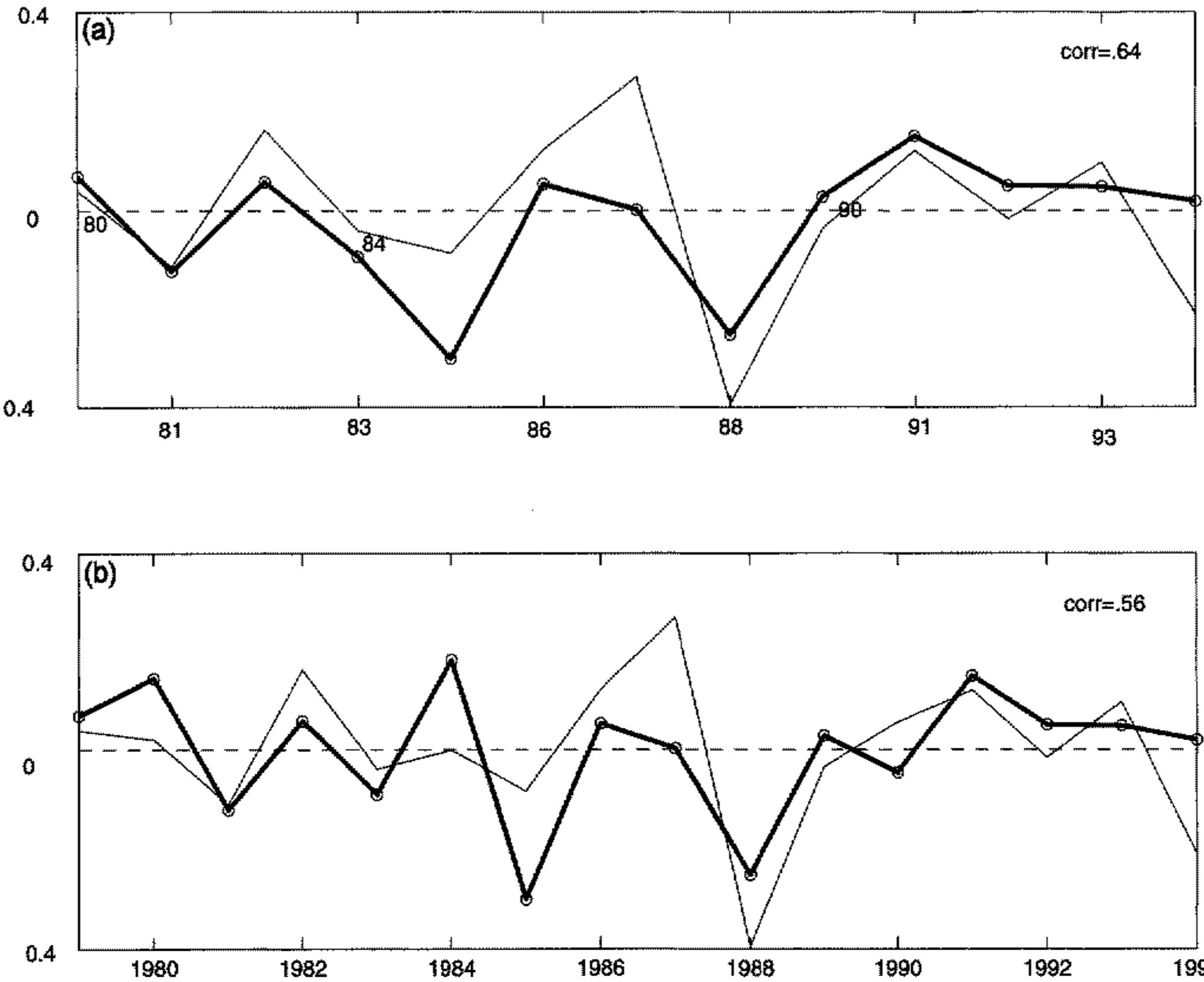

Figure 12. Same as Fig. 11, but for a four-month projection of precipitation (i.e. January(+1)) over an extratropical domain, i.e. the south-east of the USA (97.5–90.0°W, 30–30°N) from the observed Tropical-wide Oscillation Index for July–August–September. Observed precipitation is from Xie–Arkin. Including all years for which the Xie–Arkin data are available gives a correlation of 0.56. With type II elimination (1980, 1984, 1990) the correlation is increased to 0.64.

Another forecast example is the 4-month projection of precipitation anomalies for boreal winter, including parts of the extratropics. As was seen in Fig. 7(c), the ENSO effect is extended over North America, Argentina and Brazil. We take here an example of the south-east region of the United States. The association of observed precipitation in this region with the SOI during November–March was pointed out by Ropelewski and Halpert (1987) and others. This region is one of the wave-train peaks in the Pacific/North America teleconnection pattern (Horel and Wallace 1981; Wallace and Gutzler 1981). Figure 12 is the result for a small region (97.5°W–90°W, 30°–20°N). This rainfall forecast is made by the TOI(JAS), and it is verified by the Xie–Arkin precipitation. The correlations are 0.56 and 0.64 without/with type II elimination ($\varepsilon = 0.03$). In this case, the years removed are 1980, 1984 and 1990. Figure 12 suggests that the teleconnection domain is not only limited to the tropics but also extended to the extratropics.

6. Discussion and comments

(i) As has been described, it is possible to project the wet or dry monsoon from the SST of 15 months earlier. Similarly, El Niño or La Niña in the coming winters can be predicted from the information of the Indian summer monsoon intensity (correlation 0.72). But this does not necessarily mean that the latter is the cause of the former. All the elements are the constituents of the ENSO–monsoon system. The entire cause–effect

relationship holds within this framework. The major processes are the fast and slow teleconnections; the ocean plays a role in setting up the slow part of the oscillation, but acts jointly with the fast atmospheric part. The terminology 'teleconnection' is being used in this context. By the same token, the WAI indicates the transitive/intransitive processes of the ENSO–monsoon system. It is reasonable to consider that the bifurcation of type I/type II might be started near the warm pool, but the effect is quickly spread eastward at least, forming a large-scale SST distribution.

In general, the horseshoe pattern is characteristic of the SST anomalies over the Indo-Pacific Oceans. The emergence of the SST anomaly field might be related to the latitudinal difference in the propagation speeds of oceanic Rossby waves, together with the eastward faster speed of oceanic Kelvin waves. It is interesting to investigate whether this oscillation (Fig. 8) can lead to the clockwise rotation of the oceanic heat-content anomalies mentioned by Latif and Barnett (1994), and it may also be fascinating to examine whether the biennial cold waters correspond to a series of cold pulses (1976–1988), which descend into the main thermocline (at least 400 m) (Deser *et al.* 1996).

(ii) In Figs. 1 to 4 and Tables 1 and 2, a positive correlation belt was noted at JAS(0); it corresponds to the Indonesian region (120°E–160°E) with opposite sign to the other longitudes. This belt corresponds to the outer rim of the horseshoe in Figs. 6, 7, and 8. Nicholls (1984) pointed to the importance of the SST over this region for the ENSO phenomenon. Nitta (1987), based on observations, reported that the summer climate over East Asia is strongly affected by the SST near the warm pool, and that in most ENSO warm events cold SST emerges in this region; as a result, the Asian monsoons become inactive. Kawamura (1988), Sheu and Lau (1995) and Tomita and Yasunari (1996) pointed out that the South China Sea includes the large amplitude of the SST biennial oscillation, together with the Timor Sea. Ju and Slingo (1995) hypothesize that the SST anomalies in this area can influence the Asian summer monsoon, particularly the date of the monsoon onset (see Lau and Yang (1997)). The importance of SST in the Indonesian region to the TBO was noted by Meehl (1987, 1997), and the relation of upper-ocean heat content to SST in the TBO was documented by Meehl (1993).

(iii) In contrast to earlier years of ENSO research, a major focus has now been shifted from the eastern part of the basin to the western part, particularly associated with the evidence of TBO in the ocean heat content of the Mindanao Dome (5°N–12°N, 127°E–135°E) (Lindstrom *et al.* 1987; Lukas 1988; Y90; Masumoto and Yamagata 1991). This is in the warm pool, and it appears to be the area of the shallowest ocean thermocline, the thermocline ridge running longitudinally at these latitudes (see Fig. 10 of Rosati *et al.* 1994).

In sections 3(c) and (d), it was mentioned that the improvement of correlation due to type II removal is not so effective in the positive time domain. This may indicate that the major mechanism of the effect from Asian monsoon to ENSO may be different from the process related to the WAI. The phenomena affecting monsoons and thereafter triggering the El Niño have been discussed in the past 30 years. Yasunari (1979, 1980, 1981), Sikka and Gadgil (1980), and Krishnamurti and Subrahmanyam (1982) noticed that the Madden–Julian Oscillation (MJO) (Madden and Julian 1971, 1972) affects substantially the Indian monsoon rainfall. On the other hand, Kessler *et al.* (1995) studied the effect of the MJO on the El Niño in the equatorial Pacific, using the detailed observations of the tropical atmosphere–ocean array moored buoy network. They pointed out that the El Niño after 1991 at least are all triggered by the MJO, which leave from the warm pool, but the MJO is too ubiquitous to be the necessary or sufficient condition for the ENSO. The process which affects the phenomena for both oceans could be the MJO. A question is in what condition monsoon and ENSO are connected (type I) and in what condition

they are unconnected (type II). This process may or may not be the same as the shift of the Walker circulation, though the key locations for the WAI and MJO happen to be the same, i.e. the warm pool.

(iv) Examples of studies which previously found the horseshoe pattern in the SST were given at the end of section 4(b). However, we also note that the horseshoe pattern has recently emerged in the skill pattern for SST forecasts with coupled models. For example, Rosati *et al.* (1997) use 14 cases of 12-month ENSO forecasts with a coupled GCM to construct a composite map of forecast skill. The map is the SST anomaly correlation between forecast and observed, the comparison being for the 6-month period from the fourth to the ninth months, therefore excluding the initial transitional and the terminal deteriorating periods. The predictable (high correlation) areas correspond to the positive and negative high correlation areas (of the horseshoe pattern) in the teleconnection in Fig. 8, suggesting that the sequence identified in Fig. 8 may be related to predictability in ocean–atmosphere models.

(v) In this paper, experimental predictions are tested. The result suggests that forecasts require an accurate knowledge on type I/type II state and TOI(JAS). In reality, an ocean–atmosphere coupled model should be used for obtaining the information on these items. For example, to predict an ENSO from May(0) to Jan(+1), a crucial point is that the atmospheric GCM should be capable of producing a correct TOI(JAS) with appropriate cumulus parametrization and sufficient spatial resolution (see Part I), and that the air–sea GCM should be capable of predicting type II accurately in the context described in (iv) above, i.e. the warm-pool simulation.

7. Conclusions

The ENSO–monsoon system and the connection between the two subsystems were examined by using simulations of an uncoupled atmospheric GCM, and the observations. In particular, the lag correlations were investigated between the TOI and SST, vertical velocity (omega) at the 500 hPa level, precipitation, and SLP.

It is noticed that, first, the correlations are particularly strong along the Indo-Pacific equator and, at the final peak period (NDJ(+1)), there are large correlations, spreading to the extratropics and even to the Atlantic Ocean. Second, the precipitation index TOI(JAS), which has a close relation with the SOI(JAS) as well as the IMR(JAS), is a useful measure to represent the tropical teleconnection, and appears to be a more stable and robust index than the SOI(JAS) or the IMR(JJA), because the TOI(JAS) represents a broad-scale distribution of tropical rainfall. Third, this index, TOI(JAS), can be an effective precursor for SST and omega in the eastern equatorial Pacific, i.e. ENSO. Fourth, if type II cases are removed from the time sequence of ENSO–monsoon variables, the lag correlations between the TOI(JAS) and these variables are appreciably improved, so that the peak correlation climbs from 0.47 to 0.82 between TOI(JAS(0)) and the eastern tropical Pacific SST 16 months earlier (Apr(−1)), and the correlations now show distinctly the biennial character.

To summarize, the ENSO–monsoon system consists of, at least, two oscillation subsystems. These two subsystems are not annually linked but biennially linked, and they lose the link occasionally (type II) at the rate of 8 out of 34 years for the period of our study. When the SST along the equatorial Pacific (slightly south) has a climatologically stronger or weaker temperature gradient, they are linked, whereas when the SST gradient is close to normal, the connection is lost. The degree of the linkage can be estimated by an index, WAI. It appears to be the first time that this kind of view is mentioned. The increase in the linkage in type I years is much more

than would be expected by chance if near-normal values in a time series are deleted. This issue (type I/type II) is potentially very important for forecasts. The teleconnection of the ENSO–monsoon system is represented by a distinct geographical pattern of lag correlation between the TOI(JAS) and the target variables, such as omega, precipitation and SST. These patterns are characterized by the horseshoe configuration over the Indo-Pacific oceans, which is accompanied by the SPCZ-type rim and the northern hemisphere counterpart at the western side of the horseshoe (i.e. the NPCZ). The lag-correlation analysis identifies a sequence of events with the ENSO–monsoon for one phase in the boreal summer of year(−1) and for the opposite phase in the boreal summer of year(0). At that time then follows an intensification of the ENSO to a peak around NDJ(+1). The patterns (e.g. Fig. 3) look exactly biennial from boreal summer(−1) to boreal summer(0), but the whole picture is skewed by the intensification of the ENSO to NDJ(+1). Nonetheless, removing type II years, the TOI(JAS) has an exact biennial periodicity except for the 1971 case.

As was touched upon in section 4, at least two versions of the ENSO–monsoon system, i.e. (type I and type II) and (BO-type and LF-type), have been discussed. The years of type II and LF-type are not always the same years; actually only four years are common, 1958, 1968, 1977, and 1980, among eight type IIs and 11 LF-types. It is important to make this difference clear.

Acknowledgements

We would like to thank Drs Vincent Moron and Nadia Pinardi for providing various data, advice and suggestions, and Ms Elisabetta Masetti for helping with the coding of computer programs. Credit should also go to Drs Mike Davey, Jim Kinter, Uma Bhatt, J. Shukla and Larry Marx, who made various useful and important suggestions. A large portion of the figures were produced by the GrADS (the Grid Analysis and Display System), which was produced by the Center for Ocean–Land–Atmosphere Studies (COLA), and we acknowledge Mr B. Doty of COLA who taught us how to use GrADS. We gratefully acknowledge the support of the European Commission Project DICE (EV5V-CT94-0538) and (for MNW) the National Oceanic Atmospheric Administration grant NA67RJ0150 for both Parts I and II.

References

Angell, J. K. 1981 Comparison of variations in atmospheric quantities with sea surface temperature variations in the equatorial eastern Pacific. *Mon. Weather Rev.*, **109,** 230–243

Annamalai, H. 1995 Intrinsic problems in the seasonal prediction of the Indian summer monsoon rainfall. *Meteorol. Atmos. Phys.*, **55,** 61–76

Barnett, T. P. 1983 Interaction of the monsoon and Pacific trades wind system at interannual time scales. Part I. The equatorial zone. *Mon. Weather Rev.*, **111,** 756–773

1991 The interaction of multiple time scales in the tropical climate system. *J. Climate*, **4,** 269–285

Bhalme, H. N. and Jadhav, S. K. 1984 The Southern Oscillation and its relation to the monsoon rainfall. *J. Climatol.*, **4,** 509–520

Brankovic, C., Palmer, T. N. and Ferranti, L. 1994 Predictability of seasonal atmospheric variation. *J. Climate*, **7,** 217–237

Deser, C., Alexander, M. A. and Timlin, M. S. 1996 Upper-ocean thermal variations in the North Pacific during 1970–1991. *J. Climate*, **9,** 1840–1855

Gutzler, D. S. and Harrison, D. E. 1987 The structure and evolution of seasonal wind anomalies over the near-equatorial eastern Indian and western Pacific oceans. *Mon. Weather Rev.*, **115,** 169–192

Horel, J. D. and Wallace, J. M. 1981 Planetary-scale atmospheric phenomena associated with the Southern Oscillation. *Mon. Weather Rev.*, **109,** 813–829

Hsiung, J. and Newell, R. E. 1983 The principal non-seasonal modes of variation of global sea surface temperature. *J. Phys. Oceanogr.*, **13,** 1957–1967

Jiang, N., Neelin, J. D. and Ghil M. 1995 Quasi-quadrennial and quasi-biennial variability in the equatorial Pacific. *Clim. Dyn.*, **12,** 101–112

Ju, J. and Slingo, J. M. 1995 The Asian summer monsoon. *Q. J. R. Meteorol. Soc.*, **121,** 1133–1168

Kawamura, R. 1988 Quasi-biennial oscillation modes appearing in the tropical sea water temperature and 700 mb zonal wind. *J. Meteorol. Soc. Japan*, **66,** 955–965

Kessler, W. S., McPhaden, M. J. and Weickmann, K. M. 1995 Forcing of intraseasonal Kelvin waves in the equatorial Pacific. *J. Geophys. Res.*, **100,** C6, 10613–10631

Khandekar, M. L. 1979 Climate teleconnections from the equatorial Pacific to the Indian monsoon—analysis and implications. *Arch. Meteorol. Geophys. Bioklim.*, **A28,** 159–168

Kidson, J. W. 1975 Tropical eigenvector analysis of the Southern Oscillation. *Mon. Weather Rev.*, **103,** 187–196

Kiladis, G. N. and Diaz, M. F. 1989 Global climatic anomalies associated with extremes in the Southern Oscillation. *J. Climate,* **2,** 1069–1090

Kiladis, G. N. and Van Loon, H. 1988 The Southern Oscillation. Part VII: Meteorological anomalies over the Indian and Pacific sectors associated with the extremes of the oscillation. *Mon. Weather Rev.*, **116,** 120–136

Krishnamurti, T. N. and Subrahmanyam, D. 1982 The 30–50 day mode at 850 mb during MONEX. *J. Atmos. Sci.*, **39,** 2088–2095

Kutsuwada, K. 1988 Spatial characteristics of interannual variability in wind stress over the western North Pacific. *J. Climate*, **1,** 333–347

Kutzbach, J. E. 1967 Empirical eigenvectors of sea-level pressure, surface temperature and precipitation complexes over North America. *J. Appl. Meteorol.*, **6,** 791–802

Latif, M. and Barnett, T. P. 1994 Causes of decadal climate variability over the North Pacific and North America. *Science*, **266,** 634–637

Lau, K. M. and Sheu, P. J. 1988 Annual cycle, quasi-biennial oscillation, and Southern Oscillation in global precipitation. *J. Geophys. Res.*, **93,** 10975–10988

Lau, K. M. and Yang, S. 1997 Climatology and interannual variability of the south-east Asian summer monsoon. *Adv. Atmos. Sci.*, **14,** 141–162

Lindstrom, E., Lukas, R., Fine, R., Firing, E., Godfrey, S., Meyers, G. and Tsuchiya, M. 1987 The western equatorial Pacific Ocean circulation study. *Nature*, **330,** 533–537

Lukas, R. 1998 Interannual fluctuations of the Mindanao Current inferred from sea level. *J. Geophys. Res.*, **93,** 6744–6748

Madden, R. A. and Julian, P. R. 1971 Detection of a 40–50 day oscillation in the zonal wind in the tropical Pacific. *J. Atmos. Sci.*, **28,** 702–708

1972 Description of global-scale circulation cells in the tropics with a 40–50 day period. *J. Atmos. Sci.*, **29,** 1109–1123

Masumoto, Y. and Yamagata, T. 1991 Response of the western tropical Pacific to the Asian winter monsoon: the generation of the Mindanao Dome. *J. Phys. Oceanogr.*, **21,** 1386–1398

Meehl, G. A. 1987 The annual cycle and interannual variability in the tropical Pacific and Indian Ocean region. *Mon. Weather Rev.*, **115,** 27–50

1993 A coupled air–sea biennial mechanism in the tropical Indian and Pacific regions: Role of the ocean. *J. Climate*, **6,** 31–41

1994 Coupled land–ocean–atmosphere processes and south Asian monsoon variability. *Science*, **266,** 263–267

1997 The south Asian monsoon and the tropospheric biennial oscillation. *J. Climate*, **10,** 1921–1943

Mooley, D. A. and Munot, A. A. 1993 Variation in the relationship of the Indian summer monsoon with global factor. *Proc. Indian Acad. Sci., Earth & Planet. Sci.*, **102,** 89–104

Mooley, D. A. and Parthasarathy, B. 1983 Variability of the Indian summer monsoon and tropical circulation features. *Mon. Weather Rev.*, **111,** 967–978

1984 Indian summer monsoon rainfall and the east equatorial Pacific sea surface temperature. *Atmos.–Ocean*, **22,** 23–25

Navarra, A., Ward, M. N. and Miyakoda, K. 1999 Tropical-wide teleconnection and oscillation. I: Teleconnection indices and type I/type II states. *Q. J. R. Meteorol. Soc.*, **125,** 2909–2935

Nicholls, N. 1978 Air–sea interaction and the quasi-biennial oscillation. *Mon. Weather Rev.*, **106,** 1505–1508

1984 The Southern Oscillation and Indonesian sea surface temperature. *Nature*, **307,** 576–577

Nitta, T. 1987 Convective activities in the tropical western Pacific and their impact on the northern hemisphere summer circulation. *J. Meteorol. Soc. Japan*, **65,** 373–390

Ose, T., Song, Y. and Kitoh, A. 1997 Sea surface temperature in the South China Sea—an index for the Asian monsoon and ENSO system. *J. Meteorol. Soc. Japan*, **75,** 1091–1107

Penland, C. and Sardeshmukh, P. D. 1995 The optimal growth of tropical sea surface temperature anomalies. *J. Climate*, **8,** 1999–2024

Philander, S. G. H. 1990 *El Niño, La Niña, and Southern Oscillation*. Academic Press Inc., San Diego, USA

Rasmusson, E. M. and Carpenter, T. H. 1982 Variations in temperature and surface wind fields associated with the Southern Oscillation/El Niño. *Mon. Weather Rev.*, **110,** 354–384

1983 The relationship between the eastern equatorial Pacific sea surface temperatures and rainfall over India and Sri Lanka. *Mon. Weather Rev.*, **111,** 517–528

Rasmusson, E. M., Arkin, P. A., Chen, W. V. and Jalickee, J. B. 1981 Biennial variations in surface temperature over the United States as revealed by singular value of decomposition. *Mon. Weather Rev.*, **109,** 587–598

Rasmusson, E. M., Wang, X. and Ropelewski, C. F. 1990 The biennial component of ENSO variability. *J. Mar. Sci.*, **1,** 71–96

Ropelewski, C. F. and Halpert, M. S. 1987 Global and regional scale precipitation patterns associated with the El Niño/Southern Oscillation. *Mon. Weather Rev.*, **115,** 1606–1626

1989 Precipitation patterns associated with the high index phase of the Southern Oscillation. *J. Climate*, **2,** 268–284

Ropelewski, C. C., Halpert, M. S. and Wang, X. 1992 Observed tropospheric biennial variability and its relationship to the Southern Oscillation. *J. Climate*, **5,** 594–614

Rosati, A., Gudgel, R. and Miyakoda, K. 1994 Decadal analysis produced from an ocean data assimilation system. *Mon. Weather Rev.*, **123,** 2206–2228

Shen, S. and Lau, K.-M. 1995 Biennial oscillation associated with the east Asian summer monsoon and tropical sea surface temperatures. *J. Meteorol. Soc. Japan*, **73,** 105–124

Sikka, D. and Gadgil, S. 1980 On the maximum cloud zone and the ITCZ over Indian longitudes during the south-west monsoon. *Mon. Weather Rev.*, **108,** 1840–1853

Soman, M. K. and Slingo, J. M. 1997 Sensitivity of the Asian summer monsoon to aspects of sea-surface-temperature anomalies in the tropical Pacific ocean. *Q. J. R. Meteorol. Soc.*, **123,** 309–336

Sperber, K. R. and Palmer, T. N. 1997 Interannual tropical rainfall variability in general circulation model simulations associated with the Atmospheric Model Intercomparison Project. *J. Climate*, **9,** 2727–2750.

Terray, P. 1995 Space–time structure of monsoon interannual variability. *J. Climate*, **8,** 2595–2613

Thacker, W. C. and Lewandowicz, R. 1996 Climatic indices, principal components, and the Gauss–Markov theorem. *J. Climate*, **9,** 1942–1958

Tomita, T. and Yasunari, T. 1993 The two types of the ENSO. *J. Meteorol. Soc. Japan*, **71,** 273–284

1996 Role of the north-east winter monsoon on the biennial oscillation of the ENSO/monsoon system. *J. Meteorol. Soc. Japan*, **74,** 399–413

Trenberth, K. E. 1975 A quasi-biennial standing wave in the southern hemisphere and interactions with sea surface temperature. *Q. J. R. Meteorol. Soc.*, **101,** 55–74

1976 Spatial and temporal variations of the Southern Oscillation. *Q. J. R. Meteorol. Soc.*, **102,** 639–653

Trenberth, K. E. and Paolino, D. A. 1981 Characteristic patterns of variability of sea level pressure in the northern hemisphere. *Mon. Weather Rev.*, **109,** 1169–1189

Trenberth, K. E. and Shea, D. J. 1987 On the evolution of the Southern Oscillation. *Mon. Weather Rev.*, **115,** 326–332

Van Loon, H. and Shea, D. J. 1985 The Southern Oscillation. Part IV. The precursors south of 15°S to the extremes of the oscillation. *Mon. Weather Rev.*, **113,** 2063–2074

Van Loon, H. and Shea, D. J. 1987 The Southern Oscillation. Part VI. Anomalies of sea level pressure on the southern hemisphere and of Pacific sea surface temperature during the development of a warm event. *Mon. Weather Rev.*, **115,** 370–379

Verma, R. K. 1994 Variability of Indian summer monsoon relationship with global SST anomalies. *Mausam*, **45,** 205–212

Walker, G. T. 1936 'Seasonal weather and its prediction'. Pp. 117–138 in Smithsonian Report for 1935. United States Government Printing Office, Washington, USA

Walker, G. T. and Bliss, E. W. 1932 World Weather V. *Mem. R. Meteorol. Soc.*, **4,** 53–84

Wallace, J. M. and Gutzler, D. S. 1981 Teleconnections in the geopotential height field during the northern hemisphere winter. *Mon. Weather Rev.*, **109,** 784–812

Weare, B. C. 1979 A statistical study of the relationship between ocean surface temperatures and the Indian monsoon. *J. Atmos. Sci.*, **36,** 2279–2291

Webster, P. J. and Yang, S. 1992 Monsoon and ENSO: Selectively interactive systems. *Q. J. R. Meteorol. Soc.*, **118,** 877–926

Wright, P. B. 1975 'An index of the Southern Oscillation'. Climate Research Unit, University of East Anglia, Norwich, England

1985 The Southern Oscillation: an ocean–atmosphere feedback system. *Bull. Am. Meteorol. Soc.*, **66,** 398–412

Yasunari, T. 1979 Cloudiness fluctuations associated with the northern hemisphere summer monsoon over India. *J. Meteorol. Soc. Japan*, **57,** 227–242

1980 A quasi-stationary appearance of 30–40 day period in the cloudiness fluctuations during the summer monsoon over India. *J. Meteorol. Soc. Japan*, **58,** 225–229

1981 Structure of the Indian monsoon system with around 40-day period. *J. Meteorol. Soc. Japan*, **59,** 336–354

1990 Impact of Indian monsoon on the coupled atmosphere/ocean system in the tropical Pacific. *Meteorol. Atmos. Phys.*, **44,** 29–41